MASTER'S THESIS

in Atmospheric Sciences

Submitted to the

FACULTY OF GEO-AND ATMOSPHERIC SCIENCES

of the

UNIVERSITY OF INNSBRUCK

in Partial Fulfillment of the Requirements for the Degree of

MASTER OF SCIENCE

by

Markus KILIAN

Advisors

Dr. Fabien Maussion

Dr. Sabine Brinkop, Dr. Patrick Jöckel

Impact of the Eruption of Mt. Pinatubo on the chemical composition of the tropical atmosphere as simulated with EMAC

Markus KILIAN

June 15, 2018

Figure 1: Eruption of Mt Pinatubo 12. June 1991, Philippines (Copyright: R.S. Culbreth. U.S. Air Force).

Contents

Abstract

The eruption of Mt. Pinatubo on the 12 th June 1991 affected the atmosphere in the tropics (20° S - 20° N) by stratospheric heating and by a change of the heterogeneous chemistry, due to a large sulphate aerosol load. We use the EMAC model, a numerical chemistry climate model to study the impact of the eruption on the atmosphere. The sulphate aerosols are prescribed and based on satellite observations. Three different simulations were performed, namely VOL including the full volcanic perturbation, NOVOL omitting volcanic aerosols and CVOL neglecting the heating induced by volcanic aerosols. The differences between the simulations separate the temperature effect from the pure chemical effect in the stratosphere. The maximum of the volcanically induced heating is reached 4 months after the eruption at 50 hPa with 4 K. The total heating is composed of the radiative heating by stratospheric aerosols and by a change of the chemical composition. Neglecting the radiative heating by aerosols, the pure chemical effect heats the stratosphere at 10 hPa by 0.4 K and cools the lower stratosphere by 0.4 K. The total ozone column is reduced by 14 DU (6 %) within 3 months after the eruption lasting until the end of 1991. The contribution to this reduction arises primarily from the stratospheric heating by volcanic aerosols at the 20 to 50 hPa levels with 0.6 ppmv, which is 10 %. This volcanic heating increases the vertical ascent and displaces the O_3 maximum to higher altitudes. Also, the temperature increase accelerates the heterogeneous reaction rates. The pure chemical effect shows a slight increase of ozone in the first year after the eruption and a decrease in the following years. Ozone increases at 10 hPa by 0.7 ppmv (4 %). The increased aerosol surface accelerates the heterogeneous reactions, so that more NO_x is converted into HNO_3. As a result the NO_x cycle to deplete ozone slows down, and the ClO_x, HO_x and O_x cycle partly compensate the ozone depletion.

The volcanic heating increases the cold point temperature, so that stratospheric water vapour (SWV) increases by 25 %, but decreases SWV further above by an enhanced uplifting. The cooling of the lower stratosphere, due to the pure chemical effect, reduces the SWV transport by 4 %. Moreover, volcanic aerosols enhance the nucleation of water vapour to liquid and ice and subsequently decrease the SWV content. Therefore the chemical effect without the volcanic heating damps the overall SWV increase. Water vapour alters the availability of OH, which mainly determines the lifetime of methane. Therefore CH_4 increases at the beginning of the eruption above 25 hPa by up to 10 %, at those regions where less SWV is available to form OH and ozone.

This study shows that the temperature and the chemical effect of the Mt. Pinatubo eruption on the chemical composition can be separated and proved both effects to be additive. The impact of both effects on the chemical composition especially on ozone and SWV is contrary. The ozone column is reduced by the volcanic heating but slightly increases due to the chemical effect.

Abbreviations and Notations

BDC	Brewer-Dobson-Circulation
CCMI	Chemistry-Climate Model Initiative
CFC	Chlorofluorocarbons
CVOL	SC1SD-CVOL-03
DU	Dobson Unit
DKRZ	Deutsches Klimarechenzentrum
ECHAM5	European Center Hamburg Model version 5
ECMWF	European Centre for Medium-Range Weather Forecasts
EMAC	ECHAM/MESSy Atmospheric Chemistry
ERA-Interim	ECMWF Interim Reanalysis
ESCiMo	Earth System Chemistry integrated Modelling
IPCC	Intergovernmental Panel on Climate Change
MECCA	Module Efficiently Calculating the Chemistry of the Atmosphere
MESSy	Modular Earth Submodel System
MSBM	Multiphase Stratospheric Box Model
NOVOL	SC1SD-CVOL-02
PSC	Polar Stratospheric Cloud
QBO	Quasi-Biennial-Oscialltion
SAGE	Stratospheric Aerosol and Gas Experiment
SIC	Sea Ice Concentration
SST	Sea Surface Temperature
SWV	Stratospheric Water Vapour
UV	Ultraviolet
VOL	SC1SD-CVOL-01

Br	Bromine
Br^-	Bromine ion
Br_2	Molecular bromine
BrO	Bromine oxide
BrO_x	Bromine oxide family (Br, BrO)
$BrNO_3$	Bromine nitrate
CH_3	Methyl group
CH_4	Methane
Cl	Reactive chlorine
ClO	Chlorine oxide
ClO_x	Chlorine oxide family (Cl,ClO)
$ClNO_3$	Chlorine nitrate
HBr	Hydrogen bromide
HCl	Hydrochlorid acid
HNO_3	Nitric acid
H_2O	Water
HO_x	Hydrogen oxide radicals (OH, HO_2)
H^+	Hydrogen ion
HOBr	Hypobromous acid
H_2S	Hydrogen sulfide
H_2SO_4	Sulphuric acid
N_2O_5	Dinitrogen pentoxide
NO	Nitrogen oxide
NO_2	Nitrogen dioxide
NO_3	Nitrogen trioxide
NO_x	Nitrogen oxide family (NO, NO_2)
$O(^1D)$	Excited atomic oxygen
O_2	Molecular oxygen
O_3	Ozone
$O(^3P)$	Atomic oxygen
OH	Hydroxyl radical
O_x	Odd oxygen family (O,O_3)
SO_2	Sulphur dioxide

List of Figures

List of Tables

Introduction

Eruptive volcanos introduce powerful and abrupt natural forcings into the climate system. The eruption of the Mt. Pinatubo on the Philippines on the 12th of June 1991 was one of the strongest volcanic eruptions in the 20th century. The Mt. Pinatubo eruption is a well observed and studied volcano event (Thomas et al., 2009). Its eruption emitted about 20 Tg of SO_2, which penetrated the tropopause into the stratosphere. Only plumes of eruptions that are strong and explosive enough can get to those heights (von Glasow et al., 2009). Additionally, the tropical location of the Mt. Pinatubo at 15° N, triggered the rapid zonal dispersion of volcanic aerosols because the tropical upwelling and the stratospheric Brewer-Dobson-circulation provided the dynamics for a latitudinal dispersion into both hemispheres (von Glasow et al., 2009; Textor et al., 2003). Moreover, once aerosols reach the stratosphere, their lifetime extends to at least 2 years compared to 1 to 3 weeks in the troposphere. Thus, stratospheric aerosols are climate-active for a longer period of time. This long lasting climate influence is the reason - why this eruption is considered in our simulations.

The emissions of volcanic eruptions are mainly ash and sulphur in the form of SO_2, which oxidizes to sulphate in the stratosphere, and sulphate aerosols are formed within weeks. Volcanic aerosols and other non-volcanic compounds form the so-called Junge layer. It is a global aerosol layer at about 20 km altitude that reflects and scatters sunlight and regulates the temperature in the atmosphere (Telford et al., 2009). After the Mt. Pinatubo eruption, additional aerosols absorb solar radiation in the near infrared spectrum. This lead to an increase in the atmospheric extinction and therefore implied a stratospheric net heating of up to 3.5 K (Labitzke and McCormick et al., 1995), and a net cooling in the troposphere beneath of up to 0.5 K at the surface (von Glasow et al., 2009; Robock, 2000; Self et al., 1993). The heating enhanced the transport of stratospheric water vapor through the tropopause (Löffler et al., 2016; McCormick et al., 1995; Telford et al., 2009). Ozone is a well studied greenhouse gas and is also influenced by volcanic eruptions. It is of great public interest because stratospheric O_3 absorbs UV radiation and protects human health. Ozone measurements in a post-volcanic atmosphere quantified a total ozone column decrease in the volcanic plume of up to 6 % in the tropics within a month after the eruption (Schoeberl et al., 1993, Grant et al., 1992). Angell et al. (1997) reported a reduction of the total ozone column in the tropics of 2 %. The global ozone change arises from dynamic and chemical effects. Telford et al. (2009) performed three simulations with specified dynamics to separate both effects on the total ozone column. Also Muthers et al. (2015) simulated the temperature driven effects decoupled from the chemical effect with a coupled atmosphere–ocean–chemistry–climate model. Several studies have found

and investigated, that the additional aerosol surface intensifies heterogeneous reactions, e.g. converting NO_x into inactive HNO_3, provides and activates chlorine from reservoirs, and enhances catalytic ozone destruction (Solomon, 1999; Robock, 2000).

In this study, the volcanic effect due to the temperature increase and the purely chemical effect due to volcanic aerosols alone are quantified. Here the focus lies on the volcanic net effect on the ozone, methane and water vapour distribution, by means of three global chemistry-climate model simulations. The thesis is structured as follows: Chapter 1 provides the theoretical framework that is needed to interpret the research that will be conducted in this study. Chapter 2 contains the description of the chemistry-climate model EMAC and the setup of the simulations. Special attention is drawn to how the Mt. Pinatubo eruption is represented in the EMAC model. The research questions this study presents are in Chapter 3. In Chapter 4 the new findings obtained during this study are presented. Chapter 5 summarizes the major new results and discusses the volcanic perturbations of ozone and methane and put it into context with the interannual variability of other EMAC simulations. Moreover, the new findings are compared with results from the literature. In Chapter 6 conclusions by answering the research questions are made and an overview of possible expansions and improvements is given. Moreover, it highlights open questions for potential further studies.

Chapter 1

Theoretical background

1.1 Formation and Influence of Volcanic Aerosols

Large volcanic eruptions influence physical and chemical atmospheric processes in a significant way. Emitted hydrogen sulphide (H_2S) and sulphur dioxide (SO_2) react with water to sulphuric acid (H_2SO_4). Out of this, sulphate aerosols are formed, which enhance stratospheric aerosols and are rapidly zonally dispersed. This intensifies the absorption of solar radiation in the near infrared and enhances the atmospheric extinction. As a consequence, the stratosphere reacts with a net heating, the troposphere with a net cooling (Figure 1.1, Simarski, 1992). Likewise, indirect feedbacks occur after volcanic eruptions, such as an increase of stratospheric water vapour due to an intensified transport and the stratospheric heating (Löffler et al., 2016). Damped incoming solar radiation slows down the photolysis rates, which determine numerous reaction cycles (Chapter 1.2.3). Furthermore, stratospheric volcanic aerosols provide a larger surface for a multitude of heterogeneous reactions.

1.2 Basics of Atmospheric Chemistry

Von Glasow et al. (2009) highlights that the main ongoing chemical reaction in the atmosphere is oxidation, which means that all emitted sulphur will end up as sulphate and all carbonaceous compounds will finally turn into CO_2. Sulphur will be dry deposited to the ground or scavenged by aerosol particles or cloud droplets which fall onto the ground. CO_2 is absorbed by plants via the photosynthesis. The main chemical compound which causes oxidation is the hydroxyl radical OH, also called “the detergent of the atmosphere“, because it reacts with nearly all of the atmospheric gases. It develops out of water (H_2O) and the excited oxygen atom $O(^1D)$, which originates from photolysis of ozone (O_3):

$$O_3 + h\nu \longrightarrow O_2 + O(^1D) \tag{1.1}$$

$$O(^1D) + H_2O \longrightarrow 2\,OH \tag{1.2}$$

On the one hand, ozone is the precursor of OH, and a shield against ultraviolet

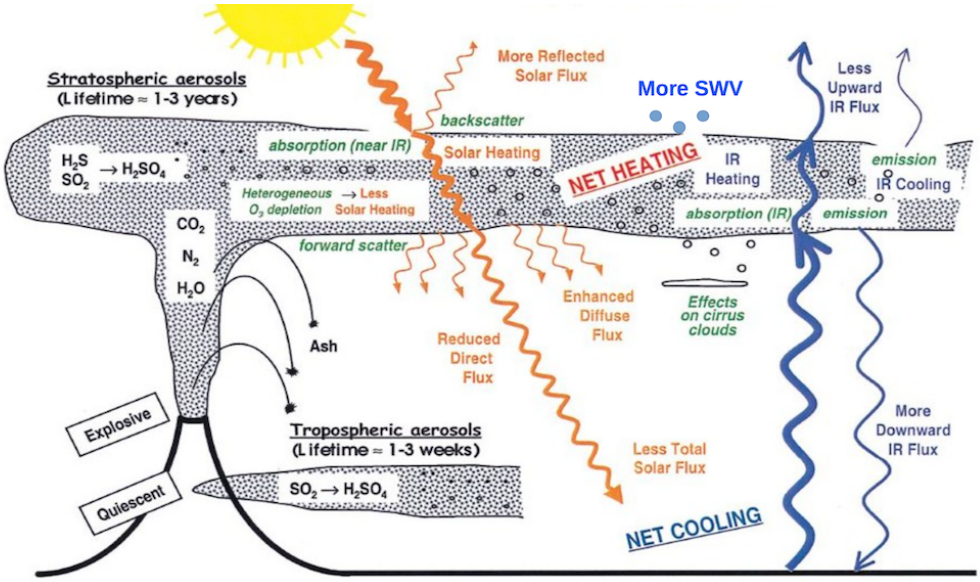

Figure 1.1: Schematic of the physical and chemical effects of a volcanic eruption on the atmosphere (Simarski, 1992; drawn by L. Walter and R. Turco; extended).

radiation and therefore serves as a protection for humanity and the biosphere. On the other hand, a high O_3 concentration near the surface is a risk for human health and vegetation. Additionally, it is a greenhouse gas and contributes to the greenhouse effect (von Glasow et al., 2009). The only source of O_3 is the photolysis of molecular oxygen, out of which atomic oxygen reacts with O_2 to O_3. This process is called Chapman cycle and is described in the following subsection.

1.2.1 Photochemical Ozone depletion and production: The Chapman Cycle

The Chapman-Cycle, discovered in 1930 by Sidney Chapman, consists of four reactions which partly explain the global distribution of stratospheric ozone. They describe the formation and the depletion of ozone, which means that this cycle keeps the ozone distribution in equilibirum. Ozone is generated by the photolysis of oxygen molecules into oxygen atoms, and by the reaction of one oxygen atom with an oxygen molecule (Middlebrock et al., 2000):

$$O_2 + h\nu \longrightarrow O + O \tag{1.3}$$

$$O + O_2 + M \longrightarrow O_3 + M \tag{1.4}$$

The produced ozone can be destroyed by photolysis followed by a reaction with an oxygen atom originating from the previous photolysis:

$$O_3 + h\nu \longrightarrow O_2 + O \tag{1.5}$$
$$O + O_3 \longrightarrow 2\,O_2 \tag{1.6}$$

Reaction 1.5 does not always destroy ozone, because the product of the photolysis is an oxygen atom, which can react with an oxygen molecule to form ozone (Reaction 1.4). The Chapman mechanism is strongly dependent on sunlight, so that the maximum ozone production can be found in the tropics. Here, ozone is produced all year around in the tropical stratosphere, but afterwards transported towards the poles via the BDC. The ozone maxima can be found at the northpole and in the southern mid-latitudes during the winter. At the poles cold temperatures form polar stratospheric clouds (PSCs), which support the polar ozone depletion (Poole and Mccormick, 1988).

In addition, the absence of solar radiation inhibits ozone production during wintertime, whereas in springtime, O_3 abruptly increases also because ozone depletion enhanced by the PSCs stops (Middlebrock et al., 2000).

1.2.2 Homogeneous Catalysis

Numerous reactions in the atmosphere are accelerated by catalysts, which in fact do not undergo a net chemical change (Atkins et al., 2006). The reaction becomes faster as the catalyst lowers its activation energy E_a and avoids the slower path of the uncatalysed reaction (Figure 1.2). Catalysts are an effective way to speed up the reaction rates of the atmospheric chemistry.

For instance, the depletion of ozone is mainly driven by catalysts. These catalytic reactions are accelerated by homogeneous catalysts, which exhibit the same phase as the reaction mixture. The catalytic ozone depletion by chlorine is a gas-phase reaction. Ozone is the reactant and chlorine the catalyst, both are in the same aggregate state (Reaction 1.11). In contrast, a heterogeneous catalyst accelerates the reaction rate of a reactant and catalyst with different aggregate states.

1.2.3 The Importance of Photolysis

Reactions in the atmosphere are often initiated by the absorption of electromagnetic radiation (Atkins et al., 2006). Photodissociation, also called photolysis, is one of the most important photochemical processes and describes the breaking of bonds in molecules by photons, as well as the production of excited molecules and radicals (von Glasow et al., 2009).

Atkins et al. (2006) points out, that the onset of dissociation can be detected in an absorption spectrum, in which the vibrational structure of a band terminates at a certain energy. Above this dissociation limit absorption occurs, thus a detection of this limit represents a way to determine the bond dissociation energy within a molecule. Thus, when a molecule gets excited to a vibrational state, the electrons experience a redistribution, which results in an internal radiationless conversion to another state.

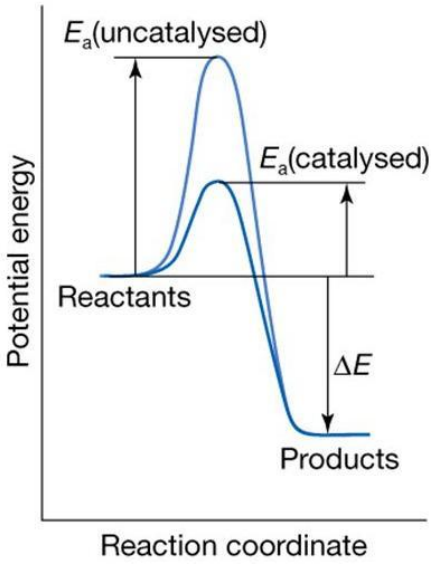

Figure 1.2: A catalyst lowers the activation energy and provides a different path. This results in an increase of the reaction rate and forms the product (Atkins et al., 2006; Figure 23.8).

The internal conversion takes place most easily at the point of the intersection of the two molecular potential energy curves because there the atomic geometries of the two states are the same (Figure 1.3). It is possible that the molecule is converted into a state that may be dissociative, which means that the states in the vicinity of the intersection have a finite lifetime (Atkins et al., 2006, Chapter 14.27). In case an incoming photon has enough energy to excite the molecule and bring it to a vibrational level high above this intersection, the described internal conversion does not take place. Should this be the case, the molecule dissociates and products are formed immediately from the excited state of the reactant (Atkins et al., 2006, Chapter 23.7). The following reaction equation describes this with

$$\mathrm{X} + \mathrm{h}\nu \longrightarrow \mathrm{Y} + \mathrm{Z}, \tag{1.7}$$

where X denotes the molecule which is dissociated by the absorption of photons, h is the Planck's constant, ν the frequency of the light wave and Y and Z are the resulting reactants. The rate of this ongoing photochemical reaction is described by the differential equation:

$$-\frac{\mathrm{d}}{\mathrm{d}t}[X] = \frac{\mathrm{d}}{\mathrm{d}t}[Y] = \frac{\mathrm{d}}{\mathrm{d}t}[Z] = k[X], \tag{1.8}$$

where k denotes the photolysis rate (s^{-1}). This rate is altitude and temperature dependent because in lower levels less UV radiation is available (Levine, 1995; Landgraf and Crutzen, 1998).
Photolysis has a strong influence on the formation of radicals which play a key role in the

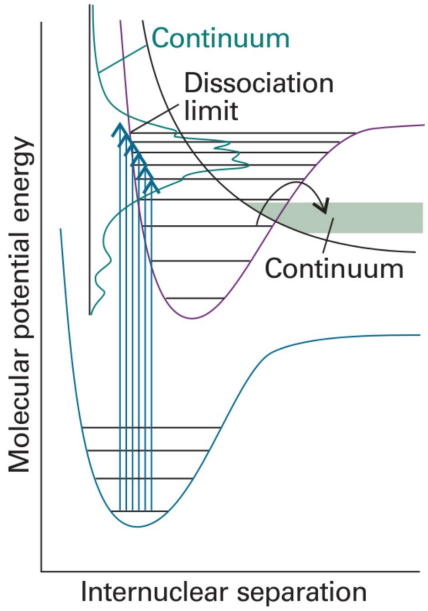

Figure 1.3: When a dissociative state crosses a bound state, as it is represented in the upper part of the figure, the excited molecules to levels near the crossing may dissociate. This process is called predissociation and identifies the spectrum, where the vibrational structure of the molecule disappears (Atkins et al., 2006).

cycles and reactions in atmospheric chemistry. In addition, it drives the Chapman cycle, as mentioned above, which produces and depletes O_3 (von Glasow et al., 2009).

1.3 The Catalytic Ozone Loss Cycles

1.3.1 The NO_x, ClO_x, BrO_x and HO_x Ozone Depletion Cycles

The depletion of ozone is not just driven by photolysis, rather stratospheric ozone can be catalytically destroyed by diverse cycles. In the early 1970s, Paul Crutzen found out, that nitrogen oxide (NO) acts as a catalyst for destroying ozone as Reaction 1.9 shows (Crutzen, 1970):

$$NO + O_3 \longrightarrow NO_2 + O_2 \tag{1.9}$$

$$O + NO_2 \longrightarrow NO + O_2 \tag{1.10}$$

Reaction 1.10 shows how the produced nitrogen dioxide reacts with an oxygen atom and forms nitrogen oxide. This ozone depletion cycle is repeated as long as NO is available for the reaction (Middlebrock et al., 2000). Nitrous dioxide does not react in the troposphere, therefore it is being able to reach the stratosphere and to react with atomic oxygen to NO (Middlebrock et al., 2000).

The sources of NO_x, namely NO_2 and NO, are anthropogenic and natural. Major anthropogenic NO_x emissions are the fossil fuel combustion and the biomass burning. In

2000, the amount of emitted NO_x was around 33 TgN/yr (Benkovitz et al., 1996). Natural sources are the emission of NO_2 by bacteria in the soil and by oceanic microorganisms. Davidson and Kingerlee (1997) estimate the contribution of soil at 21 TgN/yr. Another natural source of NO_x are lightnings, which are quantified by studies on different orders of magnitude by 12 TgN/yr (Price et al., 1997a), about 3 to 5 TgN/yr (Wang et al., 1998a) and by 2-8 TgN/yr (Schumann and Huntrieser, 2007).

In 1995, Paul Crutzen, Mario Molina and F. Sherwood Rowland have been awarded the nobel price for chemistry for their pioneering contributions to explaining how ozone is formed and depleted by chemical processes in the atmosphere (Nobel Media, 2014; Rowland and Molina, 1994). They showed how sensitive the ozone layer is in terms of anthropogenic emissions and how chlorine among other compounds is responsible for the increased ozone depletion.

Chlorine orginates not just from the exhaust of rockets and space shuttles, but Molina and Rowland found out that the main source of stratospheric chlorine oxides (ClO_x) are CFCs (Chlorofluorocarbon). They based their findings on the contributions of two other researchers.

At first, James Lovelock measured by means of a highly sensitive device that chlorofluorocarbon gases had already spread globally (Lovelock, 1971). Stolarski and Cicerone (1974) found out that free chlorine atoms in the atmosphere can deplete ozone catalytically in a similar way as nitrogen oxide (Reaction 1.9):

$$Cl + O_3 \longrightarrow ClO + O_2 \tag{1.11}$$
$$O + ClO \longrightarrow Cl + O_2 \tag{1.12}$$

Again, the produced chlorine oxide (Reaction 1.11) reacts with oxygen atoms and forms chlorine, which means that the reaction can be repeated many times as long as chlorine is available. As already mentioned, most chlorine originates from CFCs consisting of carbon, chlorine and fluorine. CFCs hardly react in the troposphere, which made them suitable for use as refrigerants, foam-blowing agents and cleaning solvents (Middlebrock et al., 2000). In the tropics, the Hadley cell transports the CFCs upward to the stratosphere. Here, they are spread to the northern and southern polar regions and contribute to the dramatic ozone loss discovered in the late 1970s - also known as the ozone Hole.

Beyond that, von Glasow et al. (2009) propose the catalytic ozone depletion due to bromine, which starts with the reaction of Br with O_3:

$$Br + O_3 \longrightarrow BrO + O_2 \tag{1.13}$$
$$BrO + BrO \longrightarrow 2\,Br + O_2 \tag{1.14}$$
$$BrO + BrO \longrightarrow Br_2 + O_2 \tag{1.15}$$
$$BrO + H_2O \longrightarrow HBr + O_2 \tag{1.16}$$

The generated bromine oxide is photolysed and the oxygen atom immediately forms O_2 together with O_3. BrO reacts with itself to reactive (Reaction 1.14) and molecular bromine (Reaction 1.15), as well as to molecular oxygen. Therefore, reaction equation 1.14 and 1.15 are the key steps in ozone depletion because they hinder the repeated formation of ozone (von Glasow et al., 2009). The major sources of stratospheric bromine arise from anthropogenic emissions, especially from industry. Natural emissions originate predominately from marine phytoplankton and volcanic eruptions, and exhibit a large variability in space and time (von Glasow et al., 2009; Hossaini et al., 2012).

The importance of the catalytic HO_x cycle for the ozone depletion was investigated by Bates and Nicolet in 1950 (Bates and Nicolet, 1950; Stenke and Grewe, 2005). The primary source of HO_x, more precisely, OH and HO_2, is the oxidation of H_2O (Reaction 1.2) and of CH_4 (Reaction 1.27). The depletion of ozone proceeds as follows:

$$OH + O_3 \longrightarrow HO_2 + O_2 \tag{1.17}$$

$$HO_2 + O_3 \longrightarrow OH + O_2 + O_2 \tag{1.18}$$

Both radicals react with ozone to molecular oxygen and the respective other radical, so that the depletion of O_3 after each reaction starts again.

1.4 Heterogeneous Stratospheric Chemistry

In contrast to the previously describe gas- and aqueous- phase chemistry, heterogeneous chemistry is the reaction of a gas on the liquid surface of an aerosol. Reaction rates of heterogeneous reactions are strongly depending on the available aerosol surface and the surrounding temperature. An abrupt increase of the aerosol surface accelerates these reactions (Seinfeld and Pandis, 1998).

1.4.1 Heterogeneous Hydrolysis of N_2O_5

The hydrolysis of N_2O_5 is the key reaction for the formation of nitric acid (HNO_3, Seinfeld and Pandis, 1998). HNO_3 is the most abundant product of heterogeneous chemistry in the stratosphere. Reaction 1.19 forms the nitrate radical NO_3:

$$NO_2 + O_3 \longrightarrow NO_3. \tag{1.19}$$

During the day, NO_3 is rapidly photolysed, but during nighttime NO_3 reacts with NO_2 to N_2O_5:

$$NO_3 + NO_2 \longrightarrow N_2O_5 \tag{1.20}$$

N_2O_5 can be photolysed back to NO_2 and NO_3 with a typical photolytic lifetime of several days at 30 km height. The final formation of HNO_3 out of N_2O_5 takes place on the surface (s) of water containing aerosol particles:

$$N_2O_5 + H_2O(s) \longrightarrow 2\,HNO_3(s) \tag{1.21}$$

During the night, the conversion of NO_2 to HNO_3 is entirely achieved on the heterogeneous pathway with reaction 1.21. During day, the photolysis of NO_3 is too fast, thus reaction 1.20 cannot take place. The formation of HNO_3 then only happens via the gas-phase reaction of NO_2 with the hydroxyl radical OH:

$$OH + NO_2 \longrightarrow HNO_3 \tag{1.22}$$

The lifetime of HNO_3 is around 10 days because HNO_3 is relatively stable. Hence, the speed of reaction 1.21 is regulated by the aerosol surface, an intensification of the aerosol layer leads to an enhanced conversion of reactive NO_x into the stratospheric reservoir (HNO_3).

1.4.2 Influence of N_2O_5 Hydrolysis on the Stratospheric Chemistry

The formation of HNO_3 together with the longer lifetime removes NO_2, which is no longer available for the catalytic NO_x cycle. This leads to a decrease of O_3 depletion via the NO_x cycle (Seinfeld and Pandis, 1998). Moreover, NO_2 regulates the formation of $ClNO_3$:

$$NO_2 + ClO \longrightarrow ClNO_3 \tag{1.23}$$

Since NO_2 decreases due to a larger aerosol surface, the conversion into $ClNO_3$ decreases as well. The same deceleration is exhibited in the reaction of bromine oxide (BrO) with NO_2, instead of ClO by forming bromine nitrate:

$$NO_2 + BrO \longrightarrow BrNO_3\,\cdot \tag{1.24}$$

Additional aerosols imply an accumulation of ClO and BrO respectively because reaction 1.23 and 1.24 slow down. However, the additional ClO and BrO molecules accelerate the catalytic ozone depletion cycles (Reaction 1.11). Seinfeld and Pandis (1998) summarize that the hydrolysis of N_2O_5 moves NO_2 from $ClNO_3$ with a 1-day lifetime to HNO_3 with a 10-day lifetime. This results in lower NO_x concentrations and a decrease in sensitivity of O_3 with respect to NO_x.

The conversion rate of NO_x to HNO_3 can be quantified by a pseudo-first-order reaction, where k_4 denotes the rate coefficient (s^{-1}):

$$k_4 = \frac{\gamma}{4}\left(\frac{8kT}{\pi m_{N2O5}}\right)^{\frac{1}{2}} A_p. \tag{1.25}$$

γ is the uptake coefficient, A_p the stratospheric aerosol surface area density, T the absolute temperature and m_{N2O5} the molecular mass of N_2O_5. Seinfeld and Pandis (1998) argue that the conversion rate of N_2O_5 to HNO_3 is most sensitive to the stratospheric aerosol surface A_p and the temperature T. This means that, the larger the temperature T and/or stratospheric aerosol surface area A_p, the more is converted to nitric acid. After a large volcanic eruption those conditions are present and increased values of A_p and T are observed.

The lifetime τ_{N2O5} of N_2O_5 is defined by

$$\tau_{N2O5} = \frac{1}{k_4}. \tag{1.26}$$

In a post-volcanic stratosphere τ_{N2O5} is smaller because the conversion rate increases.

1.5 Other relevant atmospheric species

1.5.1 Methane

Methane (CH_4) is the most abundant organic trace gas in the atmosphere, and next to water vapour and carbon dioxide the most important greenhouse gas (Wuebbles et al., 2001). Additionally, it is chemically reactive and affects the tropospheric and stratospheric chemistry.

The origins of methane emissions are natural and anthropogenic, whereupon the anthropogenic sources arise from agriculture, waste disposal, rice paddies, biomass burning, and landfills, the natural sources arise from wetlands, termites, other wild ruminants, oceans, and hydrates. In contrast to the large number of methane sources, only one major and two minor sinks for tropospheric methane exist. 90 % of the methane is removed by the hydroxyl radical OH (Chapter 1.2). The residual 10 % are removed by dry soil oxidation or transported to the stratosphere. OH forms out of photodissociated ozone and water vapour as reaction 1.2 shows. The subsequent oxidation of methane by OH is the major methane destruction reaction and proceeds as follows:

$$CH_4 + OH \longrightarrow H_2O + CH_3 \cdot \tag{1.27}$$

Furthermore, the depletion of CH_4 can take place by a reaction with chlorine (Molina and Rowland, 1974):

$$CH_4 + Cl \longrightarrow HCl + CH_3 \cdot \tag{1.28}$$

Other depletion mechanisms of CH_4 are the reaction with an excited atomic oxygen, and the photolysis by ultraviolet radiation (Ehhalt, 1967).

Chapter 2

Model Description and Method

2.1 The ESCiMo initiative

In the course of the **E**arth **S**ystem **C**hemistry **i**ntegrated **M**odeling (**ESCiMo**) initiative the MESSy Consortium performed a multitude of chemistry-climate simulations with the EMAC model for various topics, to examine climate change, ozone depletion and air quality (Jöckel et al., 2016). The EMAC model runs on the supercomputer at the Deutsches Klimarechenzentrum (DKRZ) in Hamburg. The obtained results are not only of great scientific, but also of political and social interest. The findings contribute to the WMO (World Meteorological Organization) assessment of ozone and to the IPCC (Intergovernmental Panel on Climate Change) assessment, and will help to answer research questions. The boundary conditions of the simulations can be adapt to different research questions, so that the process understanding can be improved.
This thesis is based on the analysis of three simulations computed in context of the ESCiMo project. The next section will give an overview of the technical properties of the EMAC model and describe the used model set-up for this particular case.

2.2 EMAC Model

The ECHAM/MESSy Atmospheric Chemistry (EMAC) model is a numerical chemistry and climate simulation system that includes sub-models describing tropospheric and middle atmosphere processes and their interaction with oceans as well as the influence on land and humans (Jöckel et al., 2010). The model uses the second version of the Modular Earth Submodel System (MESSy2) to link multi-institutional computer codes. The core atmospheric model is the 5th generation European Centre Hamburg general circulation model (ECHAM5, Roeckner et al., 2006). For the present study we applied EMAC (ECHAM5 version 5.3.01, MESSy version 2.52) in the T42L90MA-resolution, i.e. with a spherical truncation of T42 (corresponding to a quadratic Gaussian grid of approximately 2.8 by 2.8 degrees in latitude and longitude) with 90 vertical hybrid pressure levels up to 0.01 hPa (Jöckel et al., 2010). The applied model setup for this study comprised, among many others, the submodels MECCA and MSBM, which represent the gas-phase and heterogeneous chemistry, respectively. These submodels are important, because heterogeneous

chemistry is strongly affected by volcanic eruptions.

2.3 Model set-up

To asses the impacts of volcanic eruptions on the atmospheric chemistry by using the example of Mt. Pinatubo, in our sensitivity study we analyse 3 simulations with specified dynamics. This means, they are branched off from a specified dynamics hindcast simulation and are "nudged" with a Newtonian relaxation technique towards 6-hourly ERA-Interim reanalysis data, which originates from the ECMWF (European Centre for Medium-Range Weather Forecasts) and has been made available since 1979 (Dee et al., 2011).

Newtonian relaxation is a reasonable method to "nudge" a model's synoptic state towards the observations. The predictive equation, which includes the nudging term of variable X(t), is written as

$$\frac{\partial X}{\partial x}(t) = F(x,t) - G_x(x - \tilde{x}), \tag{2.1}$$

with the first term F representing the physics of the model and the last term representing the nudging, with $\tilde{x}$ as the analysis state and G_x as the nudging coefficient. G_x is defined by $1/\tau_x$, with τ_x denoting the relaxation time (Shao et al., 2016). This Newtonian relaxation (nudging) is applied to the prognostic variables divergence, vorticity, temperature, and the (logarithm of the) surface pressure in spectral space with relaxation times τ_x of 48, 6, 24, and 24 h, respectively. The sea surface temperatures (SSTs) and the sea-ice concentrations (SICs) are prescribed from the ERA-Interim reanalysis data and are linearly interpolated between 12 hourly values.

The nudging is not applied uniformly in the vertical: the boundary layer and the stratosphere above 10 hPa are not nudged. The nudging coefficient starts with zero at the surface and increases in the transition zone between the boundary layer and the overlying troposphere where the maximum values are reached. At 10 hPa the next transition layer begins, which means that the relaxation coefficients decrease towards zero, so nudging in the upper stratosphere does not take place (Jöckel et al., 2016).
The simulations

- SC1SD-CVOL01 (VOL)
- SC1SD-CVOL02 (NOVOL)
- SC1SD-CVOL03 (CVOL)

span the years 1989 to 1997, covering the eruption of Mount Pinatubo in June 1991. From now on simulation 1 is abbreviated by VOL, simulation 2 by NOVOL and simulation 3 by CVOL. All three simulations have the same configuration, but are different with respect to the description of volcanic aerosols and its interaction with the environment (Table 2.1). VOL represents the interactions of volcanic aerosols with both, radiation and chemistry. It is the simulation, which shows the combined influence of the Mt. Pinatubo

eruption on the atmosphere. NOVOL uses unperturbed background aerosol data, that omit additional volcanic aerosols. CVOL represents the volcanic eruption - however, only chemical reactions on the aerosol surface are affected, but radiation remains unaffected by the volcanic eruption. Thus, in CVOL the stratospheric heating by volcanic aerosols is omitted.

2.3.1 Volcanic Perturbation: Prescribed Aerosols

Chapter 1.1 pointed out the importance of volcanic aerosols for the climate system. Hence, it is of great interest to represent the aerosol layer and its perturbations in the model environment in a convenient way.
The forcing of the volcano in the model is represented by prescribed sulfate aerosols in time and space. Hence, volcanic aerosols in the model are not interactive and emitted at the location of the volcano, but rather based on measurements from satellites. This method is common, because it represents the global distribution of volcanic aerosols in time and space in an appropriate way. The aerosol data originate from the CCMI data set (Revell et al., 2017), which is based on SAGE II (Stratospheric Aerosol and Gas Experiment) extinction data. SAGE II is a satellite instrument, which provided data for the period 1960-2010. It uses a lognormal aerosol size distribution by means of the SAGE-4λ algorithm, which is compiled out of all four wavelengths (385, 452, 525, and 1024 nm) that are available in the SAGE II data set (Revell et al., 2017).

Volcanic emissions except prescribed sulfate aerosols are not considered because quantifying total volcanic emissions is rather difficult. From the extinction data and the size distribution it is possible to calculate the liquid aerosol surface area density showing the global distribution of volcanic plumes. Typical stratospheric aerosol surface area concentrations lie in the range of 0.5-1.0 μm ^{2}cm^{-3}. The Mt. Pinatubo eruption increased this value in the core of the plume up to 35 μm^{2}cm^{-3} (Grainger et al., 1995; Seinfeld and Pandis, 1998). The intensification of the liquid aerosol layer accelerates the heterogeneous chemistry (Chapter 1.4). Reaction 1.25 shows that the reaction rate k_4 is linear dependent on the aerosol surface area A_p. Figure 2.1 shows the distribution of background aerosols used in VOL and CVOL, but is omitted in NOVOL. The upper panel in Figure 2.1 shows the rapid vertical distribution of the volcano plume up to 10 hPa in the tropics between 20° S and 20° N. The highest vertical extent appeared 4 months after the eruption. The strongest increase of the liquid aerosol surface density was observed in the middle stratosphere between 20 and 70 hPa with locally more than 30 μm^{2}cm^{-3} within the plume. One year after the eruption, the major plume dropped down already to 40-100 hPa. The lower panel of Figure 2.1 shows the latitudinal dispersion of volcanic aerosols on the 30 hPa level with the highest concentrations in the tropics (20° S - 20° N). The latitudinal spread of the volcano ash arises from the tropical upwelling which transports it rapidly into the stratosphere and from the BDC, which is responsible for the poleward transport.

2.4 Methodology

The results are presented as monthly mean differences between the simulations, with exceptions being denoted clearly. The difference between VOL and NOVOL shows the combined effect of the stratospheric temperature increase due to absorption by volcanic aerosols and the intensification of the heterogeneous reactions, due to an increase of the aerosol surface density. Subtracting CVOL from VOL separates the stratospheric heating effect from the net chemical effect arising from an increase of the heterogeneous reaction rates (Table 2.1). This purely chemical effect can be separated by the differences of CVOL and VOL to omit the absorption by volcanic aerosols and the resulting stratospheric heating. Due to the applied nudging, the temporal evolution of the synoptic conditions is similar in all 3 simulations. Therefore, a one-by-one comparison shows the volcanic perturbations and a sub-synoptic noise.

Abbreviation	Simulation	Volcanic Aerosol	Aerosol Interaction
VOL	SC1SD-CVOL-01	x	Radiation, Chemistry
NOVOL	SC1SD-CVOL-02	-	-
CVOL	SC1SD-CVOL-03	x	Chemistry

Table 2.1: Overview of the three simulations with their differences in model set-up in terms of the volcanic perturbation and its interaction with the model environment.

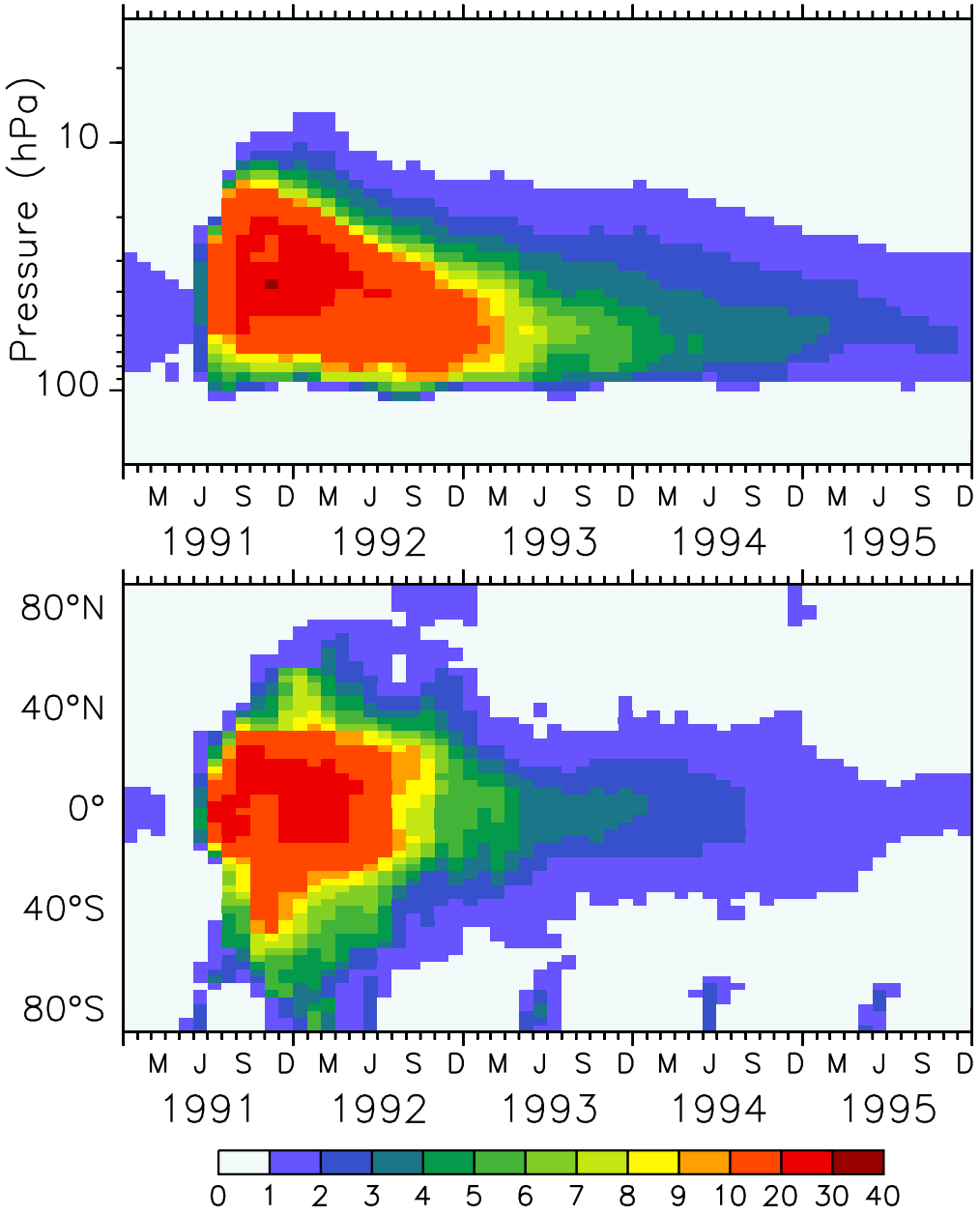

Figure 2.1: Colours show the monthly averaged liquid aerosol surface area density (10^{-8} cm^2cm^{-3}) of the volcanic sulfate aerosols in simulation VOL and CVOL in the stratosphere as tropical averaged vertical time series between 20° S and 20° N (top) and as latitudinal time series at 30 hPa (bottom). The colourbar is nearly logarithmic.

Chapter 3

Research Questions

In this study, the chemical changes in the tropical stratosphere after the Mt. Pinatubo eruption are investigated with a main focus on ozone. The amount of available data for this event is fairly good. Hence the volcanic eruption can be realistically prescribed based on observed aerosol data in the EMAC simulations VOL and CVOL. The goal is to separate the total impact of the volcanic eruption on the chemical composition of the stratosphere into the direct heating and the chemical effect arising from the larger aerosol surface. A distinction and a quantitative comparison of these two effects can not yet be found in the literature. To obtain the total effect, the interaction of prescribed aerosols with the radiation and the chemistry is fully represented in VOL. CVOL is set up to isolate the effect of the larger aerosol surface on the chemical composition, by omitting the interaction of volcanic aerosols with the radiation. The unperturbed simulation NOVOL is used as a reference and shows how the atmosphere would look like without the volcanic event.

For the first time it is possible to distinguish the effect of volcanic perturbations into a temperature and a chemical effect. Clear statements about the order of magnitude as well as the importance of each effect can be made. This leads to the following research questions:

1. How does the stratospheric heating by absorption at volcanic aerosols change the chemical composition of the tropical stratosphere?

2. How strong does the increased aerosol surface alter the chemical composition by enhanced heterogeneous reactions and how large is this effect in comparison to the temperature effect?

Chapter 4

Results

In this chapter the author systematically shows how the volcanic sulphate aerosol cloud directly and indirectly affects the atmospheric chemical composition, especially the abundance of ozone and methane (Middlebrock et al., 2000; Tie et al., 1994). Note, additional volcanic emissions are not considered and all chemical change just arise from the prescribed volcanic aerosol. The combined volcanic influence, as well as the separated temperature and chemistry effects are investigated and quantified.

4.1 Volcanic Perturbation of the Stratospheric Temperature

Sulphate aerosols increase the atmospheric extinction, resulting in a higher absorption of terrestrial (longwave) and solar (shortwave) radiation warming the stratosphere and cooling the troposphere. The strongest heating effect due to absorption is observed in the tropics because the high aerosol concentrations together with the solar radiation surplus enable this temperature rise. Volcanic heating can be directly caused by absorption at volcanic aerosols and indirectly by a change in the chemical composition, which alters solar absorption.

The upper panel of Figure 4.1 shows the combined effect of stratospheric heating (VOL - NOVOL) arising from absorption by volcanic aerosols and the changed chemical composition. The largest heating rates occur in August - one month after the eruption - in the middle stratosphere between 20 and 40 hPa. Locally, the stratosphere heated up by 0.15 K/d. Resulting from this, the greatest temperature rise takes place between August and November and finds its maximum at the end of 1991 with up to 4.0 K. It affects the lower and middle stratosphere and finds its maximum vertical extension in congruence with the plume (Figure 2.1). With the descent of the volcanic plume starting in the end of 1991, the heating is restricted more and more to the lower stratosphere. The temperature perturbation disappeared with summer 1993, in other words 2 years after the eruption.

The central panel- (VOL-CVOL) shows the direct heating due to absorption of solar radiation by volcanic aerosols only. The bottom panel displays the chemically caused

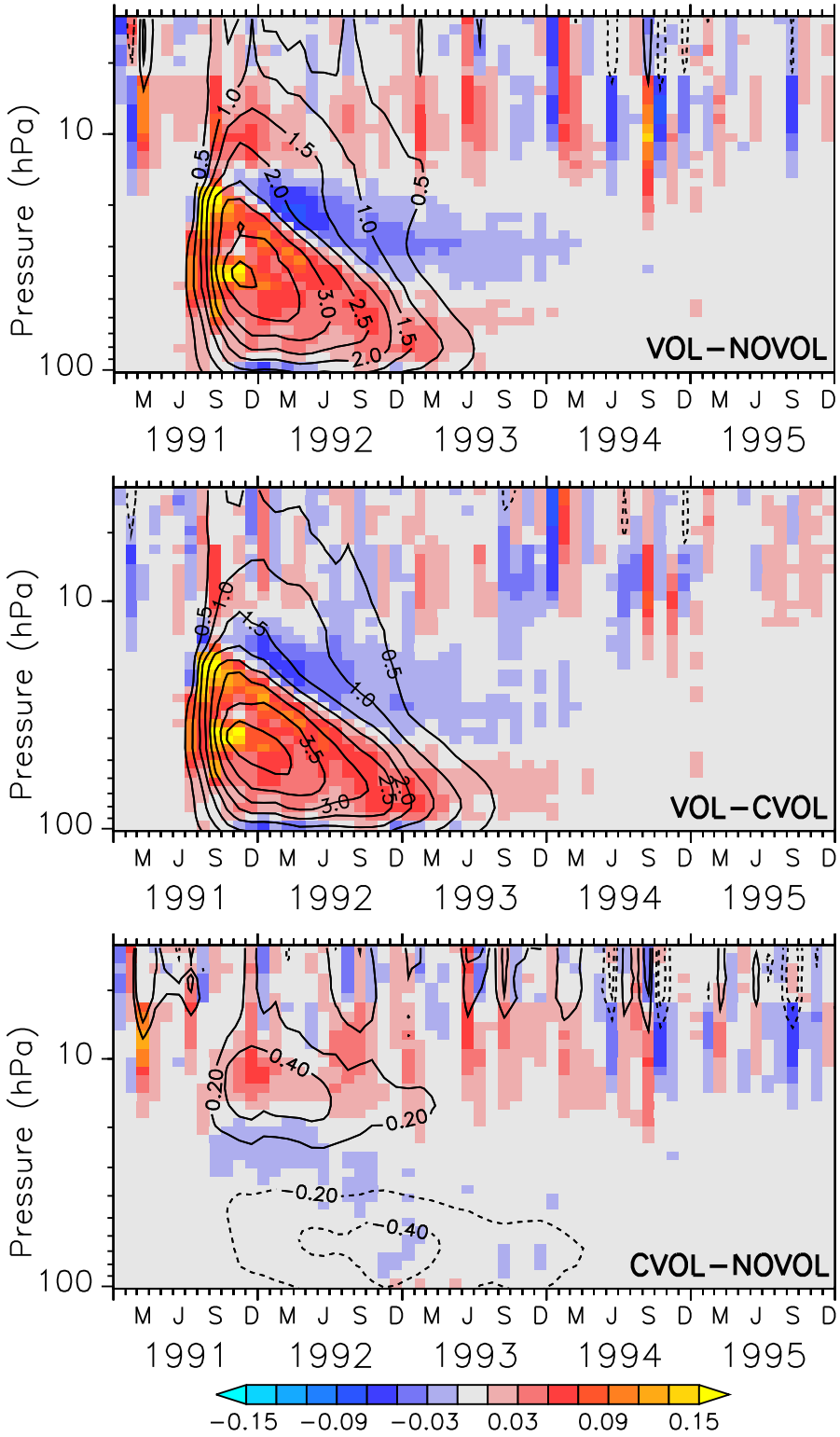

Figure 4.1: Colours show differences of the stratospheric heating rates (K/d) between VOL - NOVOL, VOL - CVOL, and CVOL - NOVOL. Contours indicate the absolute temperature change (K) induced by volcanic aerosols. Shown are tropical averages (20° S - 20° N).

change of temperature due to the changed chemical composition. It results in a heating in the upper stratosphere between 5 and 20 hPa of 0.4 K and a cooling between 30 and 70 hPa in the same order of magnitude.

The heating rates in the bottom panel of Figure 4.1 correspond to the stratospheric ozone perturbation explained in the next section. More stratospheric ozone increases temperature by more absorption of solar radiation and less ozone cools the stratosphere. The main temperature change of this volcanic eruption arise from the radiative properties of volcanic aerosols and less from the absorption of modified ozone. Overall, the volcanic heating in the middle stratosphere is slightly damped by the ozone decrease. This change of the chemical composition will be quantified in the next section.

4.2 Effects of Volcanic Aerosols on Stratospheric Ozone in the Tropics

4.2.1 Global mean unperturbed distribution of Ozone

Ozone has a strong seasonal, spatial and vertical variability, which is mostly driven naturally, but also anthropogenic. Vertically, ozone increases with height and forms in the upper stratosphere between 5 and 20 hPa the ozone layer with a mixing ratio of 10 to 12 ppmv (Figure 4.4, left panel). Most of the ozone mass shown as the ozone concentration is located further below between 15-30 hPa (Figure 4.2). Figure 4.3 shows the mean total ozone column in DU for the period 1991-1995. It becomes apparent that the lowest total ozone column values with 270 DU appears in the tropics, where the annual variation of ozone is mostly marginal. Even though the highest surplus of UV radiation and thus ozone production occurs in the tropics, the surplus of O_3 is transported towards the poles by the BDC.

The polar regions show the strongest annual variation with the largest values of up to 450 DU in winter and early spring at the North Pole and the lowest values of down to 140 DU at the South Pole during the southern hemisphere spring. The minimum over Antarctica is the well-known ozone hole, which results from anthropogenic emissions and was discovered in the beginning of the eighties (Farman et al., 1985). The main focus of the present study, however, lies on the tropical region between 20° S and 20° N.

4.3 Evaluation of Stratospheric Ozone

In order to evaluate the reliability of the simulated ozone distribution, the volcanic simulation VOL is compared to the SWOOSH (Stratospheric Water and OzOne Satellite Homogenized) data set provided by from NOAA (National Centers for Environmental Information). This data set was constructed to investigate the variability and change in water vapour and ozone in the stratosphere (Davis et al., 2016). SWOOSH is a database of global long-term satellite O_3 and SWV measurements presented on a vertical grid as monthly averages on pressure levels. The data from different satellite instruments, namely

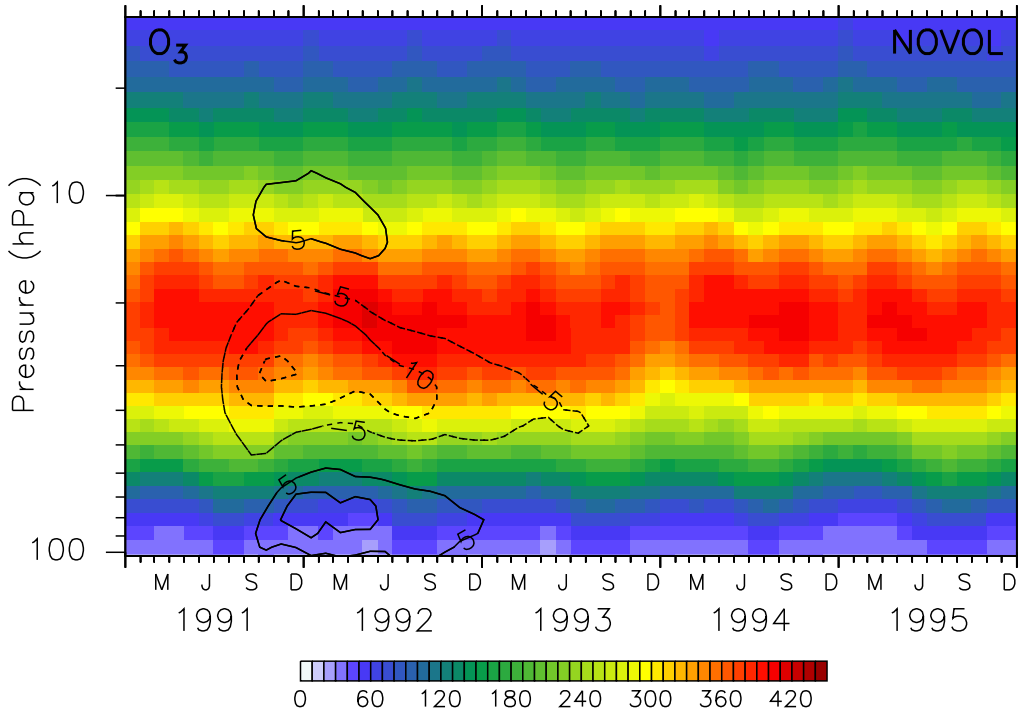

Figure 4.2: Colours show zonally averaged absolute vertical ozone concentration (μgm^{-3}) in the tropics (20° S - 20° N) in the unperturbed simulation NOVOL (colours). Contours represent the volcanically caused ozone change in VOL relative to the absolute values (%) of NOVOL. Contour intervals are 5 %.

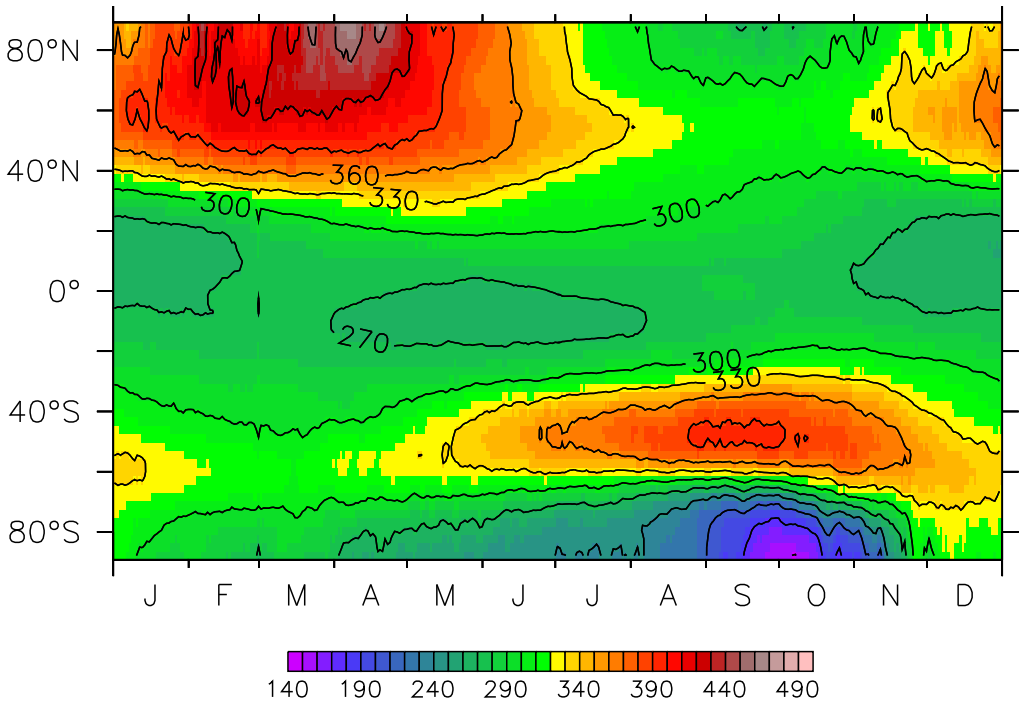

Figure 4.3: Colours show the zonally averaged climatological daily mean of total ozone over the vertical column (DU) for the period 1991 - 1995. Contours indicate the absolute values of the unperturbed simulation NOVOL.

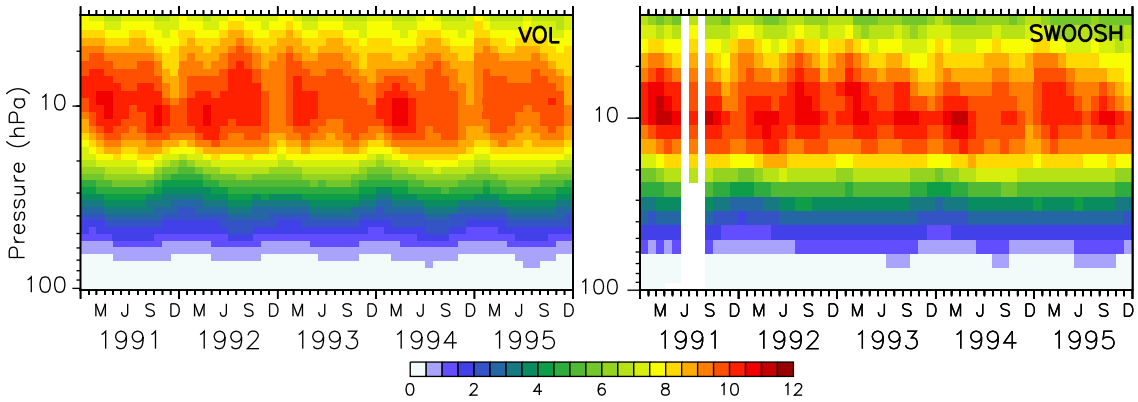

Figure 4.4: Colours show the absolute zonally and monthly averaged ozone mixing ratios (ppmv) at 10° N of the volcanic simulation VOL and the SWOOSH data set for the period from 1991-1995.

SAGE II, SAGE III, HALOE, UARS MLS and EOS Aura MLS, as well as from other merged data products has been combined.

The spatial distribution of the absolute ozone in NOVOL convincingly corresponds to the SWOOSH data (Figure 4.4). The ozone layer between 5 and 20 hPa with mixing ratios of 10-12 ppmv is well represented. The annual variation of O_3 is just partially presented in the SWOOSH data set, because the grid resolution is much coarser than in VOL. Nevertheless, the ozone maximum at 10 hPa in summer 1991 is in the SWOOSH data well represented. With the Mt. Pinatubo eruption in June 1991, the atmosphere was too opaque for reliable satellite measurements, and consequently, those months are marked with white stripes showing the data gap. All in all, the distribution of O_3 in VOL seems to be useful and reliable in terms of magnitude and location.

4.3.1 Ozone Perturbation

The ozone perturbation due to the volcanic eruption shows a pattern with an ozone increase in the upper and lower, and an O_3 decrease in the middle stratosphere (Figure 4.5, upper panel). These changes arise from a combination of the volcanic heating by aerosols and the temperature change due to the altered chemical composition. The ozone increase starts in September 1991 with 0.8 ppmv at 10 hPa which is more than 10 % of the absolute value. Between 20-50 hPa an ozone decrease of 0.7 ppmv can be observed. This is a local reduction of up to 15 %. In the lower stratosphere another increase of ozone of up to 10 % occurs. This O_3 increase is purely caused by the volcanic heating (central panel). Also, the reduction of O_3 of 10 % is mostly caused by the direct heating effect by volcanic aerosols. It increases the vertical ascent by 20 % (Dameris et al., 2005) and displaces the O_3 maximum to higher altitudes. Next to the dynamical influence, the volcanic heating increases the heterogeneous reactions rates and slightly alters the O_3 chemistry. The ozone gain at 10 hPa is induced by the chemical effect of the enhanced heterogeneous chemistry with 4 % (lower panel). Also, the lower half of the stratosphere is affected by the chemistry with an O_3 decrease, which damps the O_3 increase produced by the direct volcanic heating. Interestingly, the perturbation of ozone ends in summer 1994 and therefore lasted one year

longer than the temperature perturbation (Figure 4.1). The pure chemical change of ozone is induced by the additional surface of aerosols, which intensifies heterogeneous reactions. Larger aerosol surfaces lead to a reduction of NO_x into inactive HNO_3, and similarly as described by Solomon (1999) this liberates chlorine and bromine from reservoirs and enhances catalytic ozone destruction (Solomon, 1999; Robock, 2000; von Glasow et al., 2009). The reduction of NO_x produces an imbalance and shifts the chemical equilibrium. Moreover, heterogeneous reactions of NO_x are temperature dependent. This fact becomes important in attempting to explain the ozone anomalies due to stratospheric warming.

By integrating the whole ozone column, the combined effect consisting of the chemical and temperature driven change on the total O_3 is obtained (Figure 4.6, upper panel). Overall, the zonally averaged total ozone column in the tropics decreases by 6 % starting in August 1991. The absolute change become most pronounced between the equator and 10° S with more than 10 DU. This negative anomaly caused by the volcanic eruption appears again one year later in summer 1992, but further south.
All in all, it took 2 years until the negative ozone perturbation disappears from the northern hemisphere and after 3 years, from the southern hemisphere. Inspite of Mt. Pinatubo being located at 15° N, the strongest ozone anomaly occurs south of the equator because during southern hemispheric winter and spring, the BDC is enhanced. With December 1991, this peak shifted to the north and larger temperature gradients intensify the northern directed BDC. These negative anomalies arise mostly from the direct volcanic heating because the pure chemical effect of the volcano exhibits only a small positive perturbation of 2 DU beginning in August 1991 (bottom panel). The strongest chemical effect can be observed exactly one year later between 10° and 20° S with a decrease of up to 4 DU. This shows that the total ozone changed one year later until this positive anomaly turned into a decrease. The total ozone changes mostly as an effect of volcanic heating and the subsequent acceleration of the heterogeneous chemistry.

4.3.2 Perturbation of the Ozone Depletion Catalysts

4.3.2.1 NO_x

The unperturbed distribution of stratospheric NO_x exhibits an increase in height, with values of 1 ppbv in the lower and 18 ppbv in the upper stratosphere (Figure A.1). The combined effect of the volcanic perturbation of NO_x shows a clear decrease with the highest absolute values at the top edge of the plume (Figure 4.7, upper left panel). Between 20-30 hPa NO_x is relatively more than cut into half. The direct volcanic heating has a small loss contribution to this decrease with 20 % (central left panel). This reduction is, however, not caused by formation of HNO_3 out of NO_x, because HNO_3 decreases. At this temperature regime NO_x is transferred into other reservoir gases like $ClNO_3$ and $BrNO_3$ (Reaction 1.23 and 1.24). The reduction of NO_x due to the pure chemical effect is caused by a speed up of reaction 1.21, which transfers NO_x into HNO_3 (Figure 4.7, lower right panel).

HNO_3 is a reservoir gas with a relatively long lifetime and stores reactive NO_x. Overall after the eruption, HNO_3 shows an increase, with the largest absolute values of up to 1 ppbv at 10 hPa. This change corresponds to about 50 % in the upper stratosphere and 30 % in

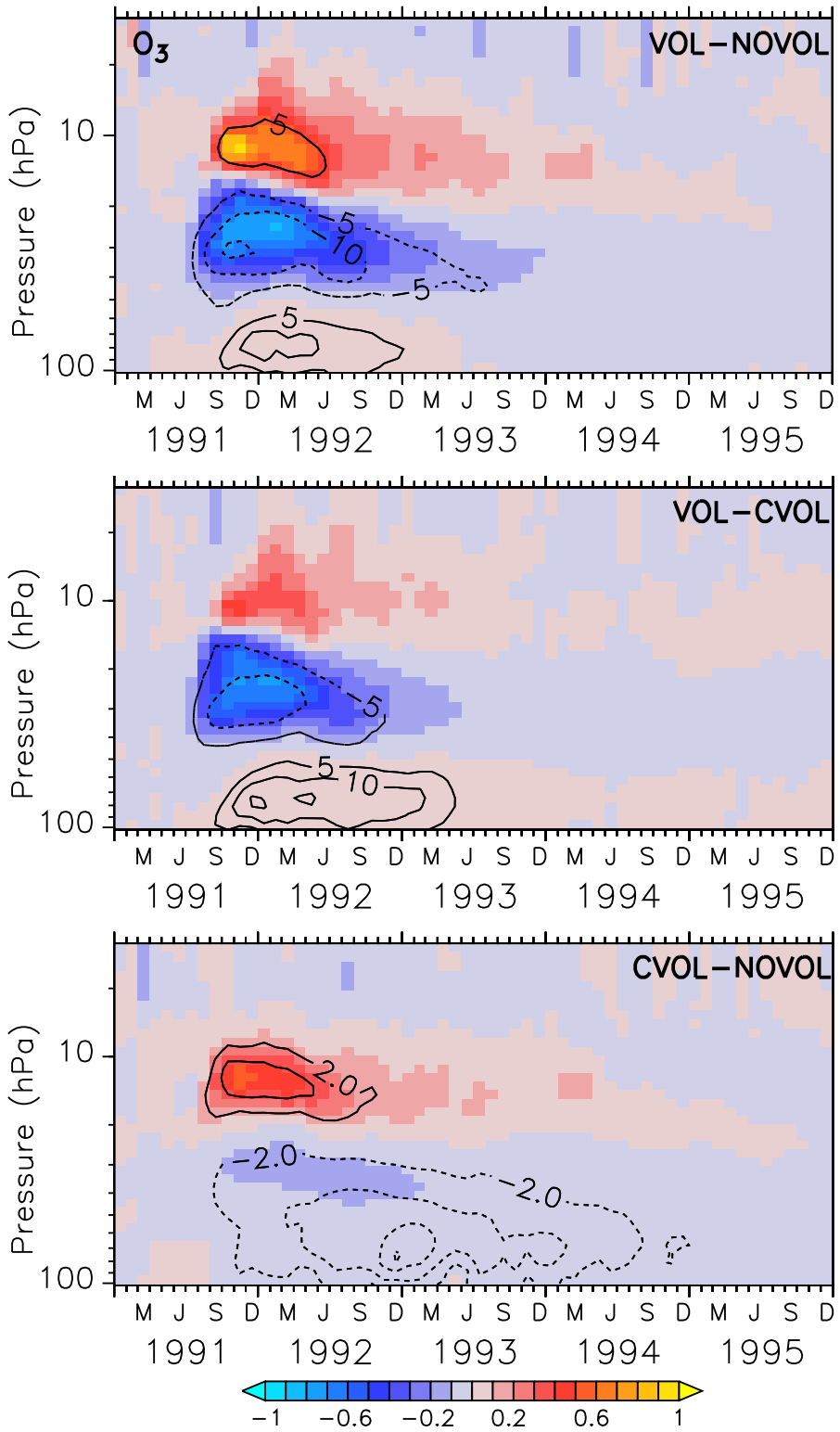

Figure 4.5: Colours show the zonally averaged absolute differences of ozone mixing ratios (ppmv) between the simulations. Contours indicate the corresponding relative changes (%). Shown are tropical averages (20° S - 20° N). Contour intervals are 5 % in the upper and central panel, and 2 % in the bottom panel.

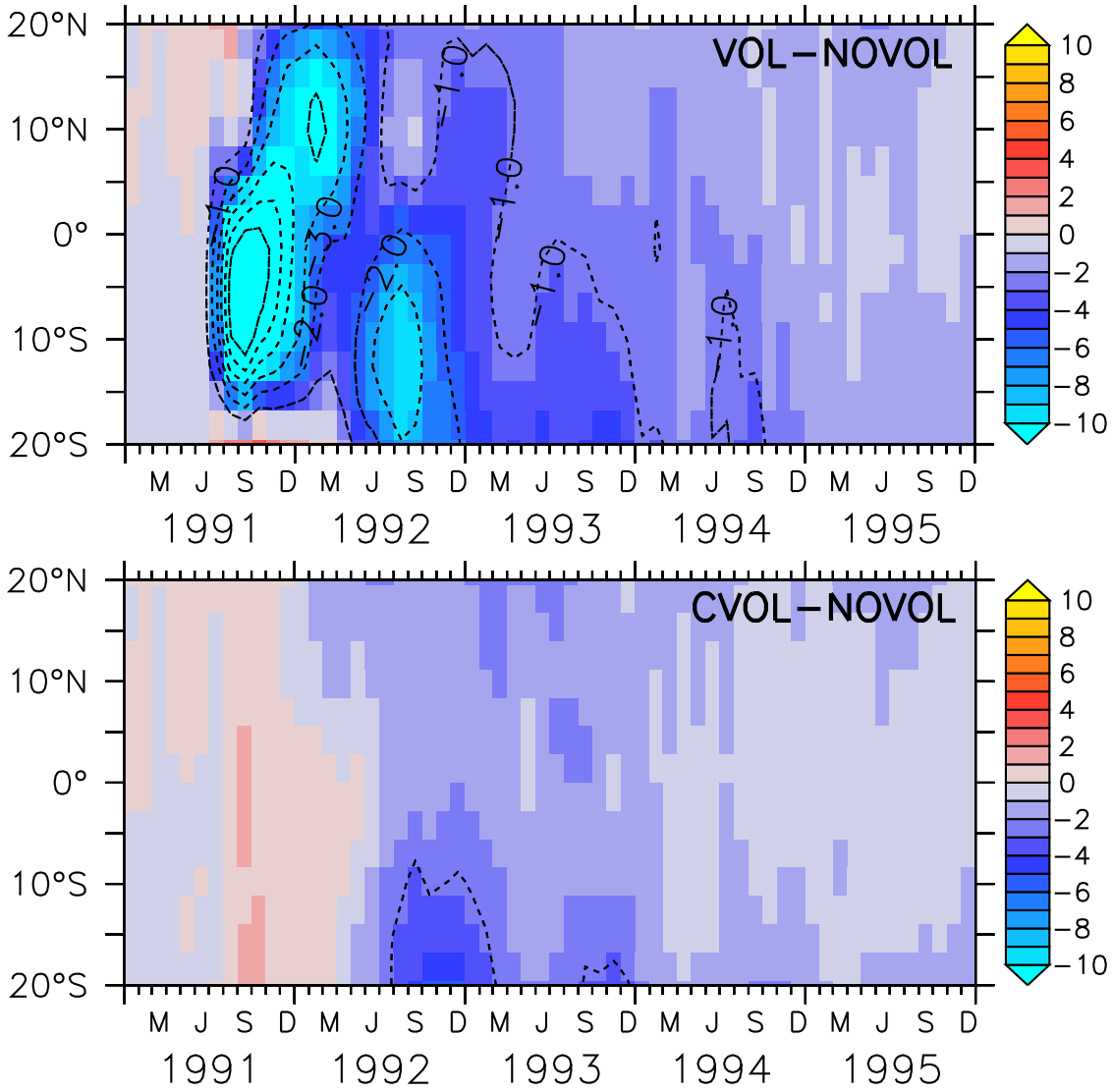

Figure 4.6: Colours show the absolute differences of the monthly zonal mean total ozone column (DU) of VOL-NOVOL (upper panel) and CVOL - NOVOL (lower panel) from 1991 - 1995. Contours indicate the corresponding relative changes (%). Contour intervals are 1 %.

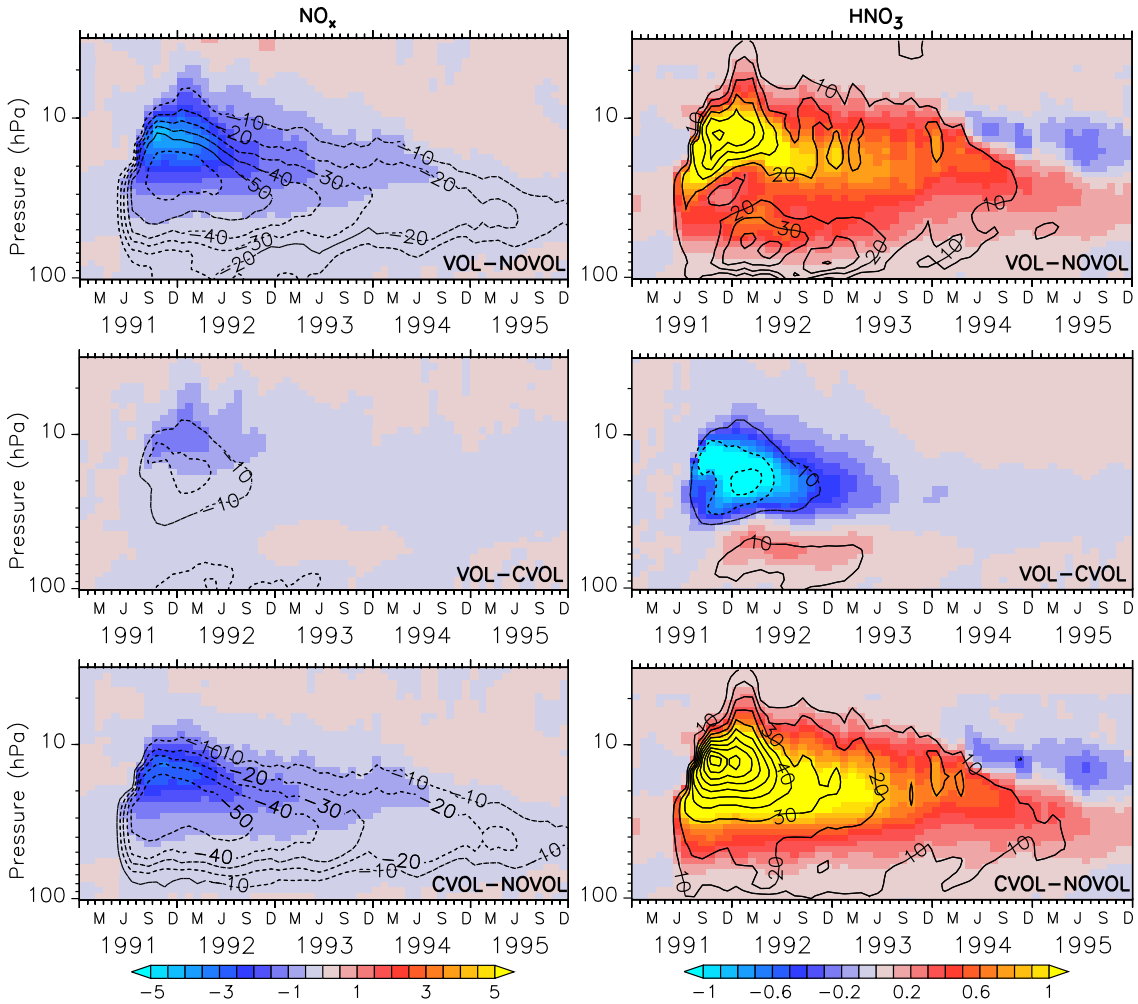

Figure 4.7: Colours show the absolute differences of NO_x (left) and HNO_3 (right) mixing ratios (ppbv) between the simulations. Contours indicate the relative percentage (%) change due to the volcanic eruption in the tropics. The contour interval is 10 %. All values are zonally and latitudinally averaged between 20° S and 20 ° N.

the lower stratosphere (Figure 4.7, upper right panel). The direct volcanic heating reduces HNO_3 between 10-30 hPa. The strongest increase of HNO_3 comes from the pure chemical effect, which takes place on the aerosol surface and enhances the transformation of NO_x into HNO_3. Here, up to 130 % more HNO_3 is produced. Hence, the loss of HNO_3 due to the volcanic heating damps the increase of HNO_3. The changes of NO_x due to the heating can be explained by the temperature dependence of the heterogeneous reaction rates. The heterogeneous reaction rates of reaction 1.21 are already accelerated by up to 1.5 % at a heating of 3 K. The biggest contribution to the NO_x and the HNO_3 reduction comes from the pure chemical effect due to the enlarged aerosol surface with up to 50 % and 130 %, respectively . The increased liquid aerosol surface accelerates the heterogeneous reaction rates and reduces NO_x.

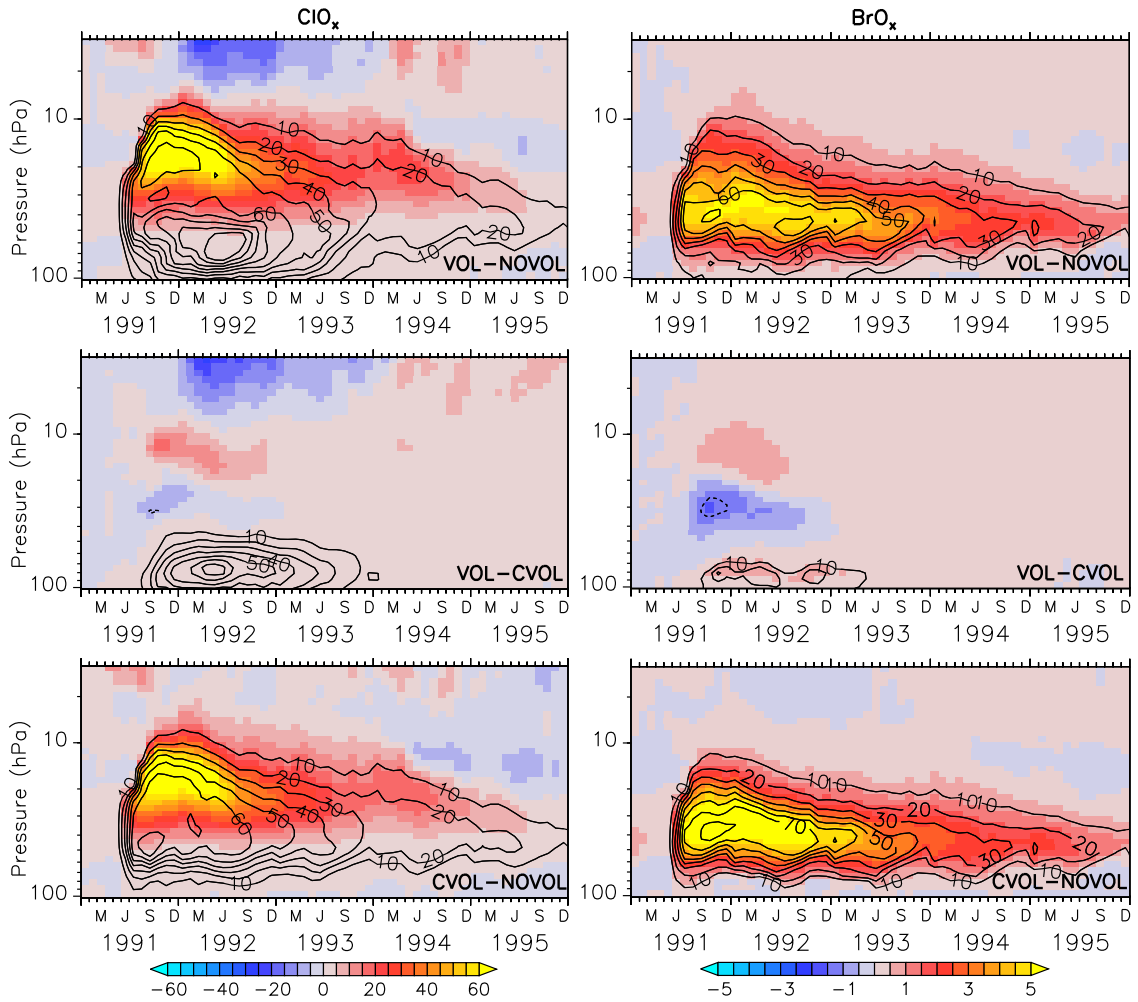

Figure 4.8: Colours show the vertical time series of the absolute differences of ClO_x on the left and BrO_x mixing ratios on the right (pptv). Calculated for the combined (VOL-NOVOL), the temperature (VOL-CVOL) and the chemical effect (CVOL-NOVOL). The mixing ratios are represented as monthly, zonally and tropical averages between 20° S and 20° N. Contours indicate the relative change (%) of the catalysts mixing ratio, triggered by the volcanic perturbation. Contour intervals are 10 %.

4.3.2.2 ClO_x

The unperturbed distribution of ClO_x increases with height and lies within the order of magnitude of 20 pptv in the lower stratosphere and 200 pptv at 10 hPa (Figure B.1). In comparison to NO_x, the abundance of ClO_x is two orders of magnitudes lower. The combined effect of the volcanic perturbation of ClO_x shows an increase with the highest absolute values again at the top edge of the plume (Figure 4.8, upper left panel). The relative change at 20 hPa is 60 %, in the lower stratosphere of up to 100 %.

The strong relative increase of ClO_x in the lower stratosphere is caused by the volcanic heating, but compared to the absolute mixing ratios at this height it is of less importance. The major gain of ClO_x can be attributed to the change in the chemistry, which alters heterogeneous reactions. In general, the stratospheric heating has less influence on ClO_x

and NO_x compared to the enlargement of the liquid aerosol surface. Changes in ClO_x and NO_x are anti-correlated. Everywhere, where NO_x is reduced, ClO_x reacts with an increase. This arises from the chemical relation of both catalysts. If less NO_x is available due to the storage in HNO_3 reaction 1.23 slows down. It forms $ClNO_3$ out of ClO and NO_2. Hence, more ClO_x remains available and becomes photolysed into reactive Cl to run the catalytic ozone depletion (Reaction 1.11). Overall, reaction 1.21 and 1.23 are accelerated by the volcanic heating and by the larger liquid aerosol surface. This forms, the pattern of the NO_x and ClO_x anomalies.

4.3.2.3 BrO_x

The abundance of stratospheric bromine oxide is small in comparison to NO_x and ClO_x and lies between 5 and 10 pptv in the relevant region of the volcanic plume (Figure C.1). It slightly increases with height. BrO_x exhibits a strong increase immediately after the eruption within the volcanic plume, locally up to 80 % (Figure 4.8, upper right panel). The direct volcanic heating causes a small reduction of BrO_x of 2 pptv, which corresponds to 10 % between 20-50 hPa, and an in increase at 10 hPa and in the lower stratosphere of locally 20 %.

The overall effect of BrO_x is slightly damped by the temperature effect by a decrease of BrO_x up to 10 % in the middle stratosphere. The major increase occurs within the volcanic plume and is purely caused by the larger aerosol surface. BrO_x is the way it forms with ClO_x, $BrNO_3$, comparable with NO_x (Reaction 1.24). The enhancement of the liquid aerosol surface causes an acceleration of the reactions. BrO_x is again affected by the NO_x reduction and photolysed into reactive Br, which becomes than available to deplete catalytically ozone.

4.3.2.4 HO_x

The HO_x cycle depletes O_3 via the HO_2 and the OH radical (Reaction 1.17 and 1.18). The vertical distribution of HO_x is altitude dependent and increases from 5 pptv in the lower to 100 pptv in the upper stratosphere (Figure D.1). The absolute abundance of HO_2 is a few orders of magnitudes larger than of the OH radical.

The perturbation of OH is comparatively small compared to HO_2 (Figure 4.9), which contributes the largest change of the HO_x cycle. The combined effect shows a clear increase of HO_x between 5-20 hPa (Figure 4.9, upper left). Next to the largest absolute changes, relative changes of up to 30 % occur, whereas in the lower stratosphere relative changes of 80 % dominate. The volcanic heating caused a small increase in the upper and a relative increase of 40 % in the lower stratosphere. The largest perturbation of HO_x is caused by the larger aerosol surface alone (bottom left). The largest relative changes of HO_x up to 90 % occurs in the lower stratosphere.

The largest perturbation of OH due to the combined effect is 10 % in the lower stratosphere (Figure 4.9, upper right panel). The volcanic heating reduces OH between 5-20 hPa about 0.5 pptv, which corresponds to 6 %. This seems to originate from the

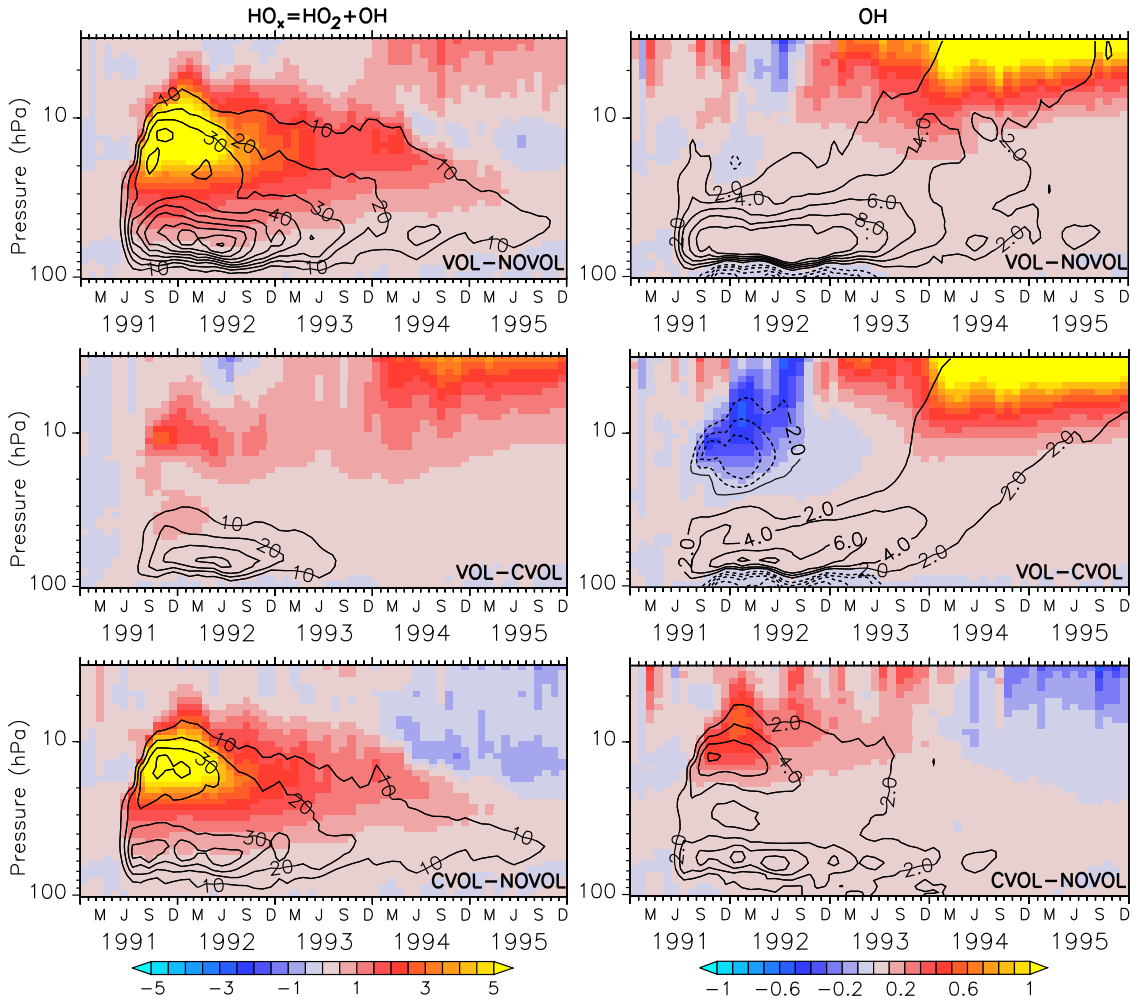

Figure 4.9: Colours show a vertical time series of the absolute differences of the HO_x mixing ratios on the left and OH mixing ratios on the right (pptv). Calculated for the combined (VOL-NOVOL), the temperature (VOL-CVOL) and the chemical effect (CVOL-NOVOL). The mixing ratios are represented as monthly, zonally and tropical averages between 20° S and 20° N. Contours indicate the relative change (%) of the catalysts mixing ratio, triggered by the volcanic perturbation. Contour intervals are 10 %.

decrease of the SWV in this region. In the lower stratosphere, OH increases due to the increase of SWV transport into because this anomaly propagates upwards with time. OH is formed out of $O(^1D)$ and water vapour, so that especially change in H_2O alter the production of the hydroxyl radical. Additionally, the higher O_3 concentration in this area accelerates reaction 1.6, so that more $O(^1D)$ is available to form OH.

The same behaviour is caused by the chemical effect, which shows an increase of OH by 0.6 pptv corresponding to 6 % at 10 hPa (lower right panel). Altogether, the volcanic heating perturbs OH in the same order of magnitude to the chemistry, but with an opposite sign. This explains the close to zero values of OH for the combined effect (VOL-NOVOL).

Since, the volcano clearly affects the catalytic cycles, the following section investigates the spatial and quantitative changes.

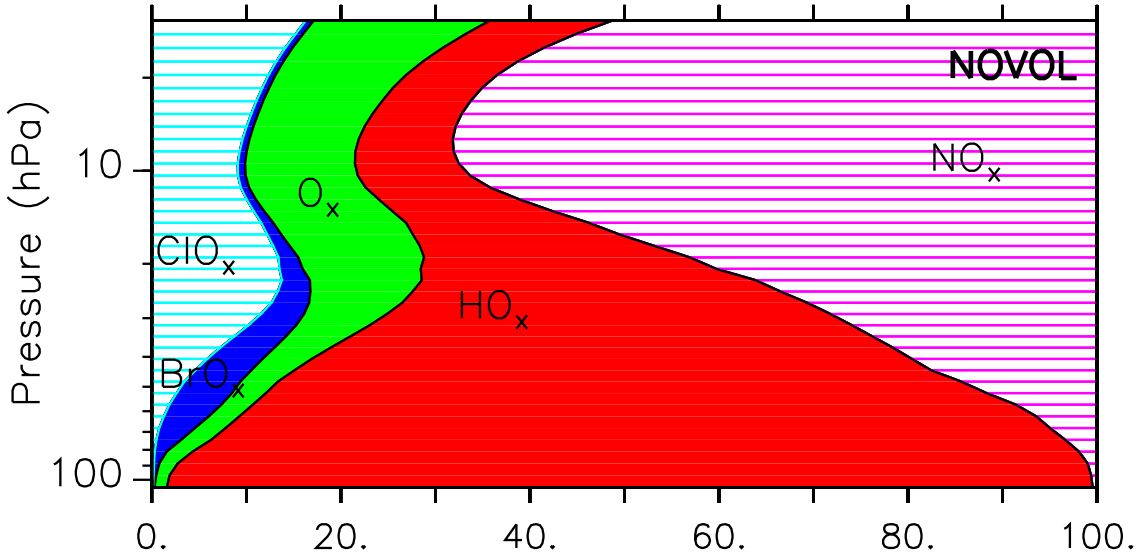

Figure 4.10: Colours show the relative contribution (%) of the individual catalytic ozone loss cycles to the total ozone loss for the unperturbed simulation NOVOL as a zonally and tropical averaged time series between 20° S and 20° N.

4.3.3 Contribution of the Catalytic Cycles to the Ozone Depletion

In the Chapman cycle O_3 is depleted through photolysis and through catalysis. The different catalytic cycles in NOVOL have their maximum impact at different heights (Figure 4.10). The influence of the NO_x cycle increases strongly with height and contributes 70 % to the overall ozone loss at 10 hPa. The contribution of the HO_x cycle has its maximum at 100 hPa with almost 100 %, and its lowest contribution at 10 hPa with 10 %. In the tropics, the abundance of water vapour is relatively larger compared to the mid-latitudes. ClO_x has its maximum at 20 hPa in the upper stratosphere with a relative contribution of 17 %. The contribution of the Chapman cycle to the ozone depletion, here denoted as O_x, increases with height. BrO_x has the lowest contribution with 1 to 5 %, with the largest impact in the lower stratosphere.

4.3.4 Change of the relative Contributions of the Catalytic Ozone Depletion Cycles

The Mt. Pinatubo eruption caused a shift in the contribution of the different catalytic cycles. The combined volcanic effect shows a strong reduction of the NO_x cycle contribution of 17 percentage points between 10 and 20 hPa (Figure 4.11, upper panel). All other catalytic ozone depletion cycles become intensified with mostly 5 to 8 percentage points of increase. The impact of O_x increases at 10 hPa, where O_3 exhibits an increase of 5 %. Larger concentrations of O_3 imply, that more O_3 is available for the Chapman reaction 1.6 to deplete ozone. ClO_x and HO_x show an increase in the ozone loss in the middle stratosphere by 6-8 percentage points.

7 % of the reduction of the NO_x cycle arise from the volcanic heating (middle panel).

The small ozone increase by the temperature effect at 10 hPa accelerates ozone depletion through the O_x cycle by 3 %. The impact of HO_x increases by the same order of magnitude at 30 hPa. The largest contribution to the changes of the catalytic cycles is caused by the larger aerosol surface and the altered chemical equilibrium (lower panel). Here, the impact of the NO_x cycle decreased by 14 % at 20 hPa, so that the ClO_x and HO_x cycles enhance both by 7 %. The increase of the O_x cycle occurs at the same magnitude as in the case of the volcanic heating. The BrO_x cycle slightly increases by 2 % at 60 hPa. As soon as the NO_x cycle is perturbed and decreases, all other catalytic cycles react with an increase to compensate the chemical imbalance.
It can be noted that the acceleration of the heterogeneous chemistry affects the catalytic O_3 depletion stronger than the volcanic heating due to the additional aerosol surface.

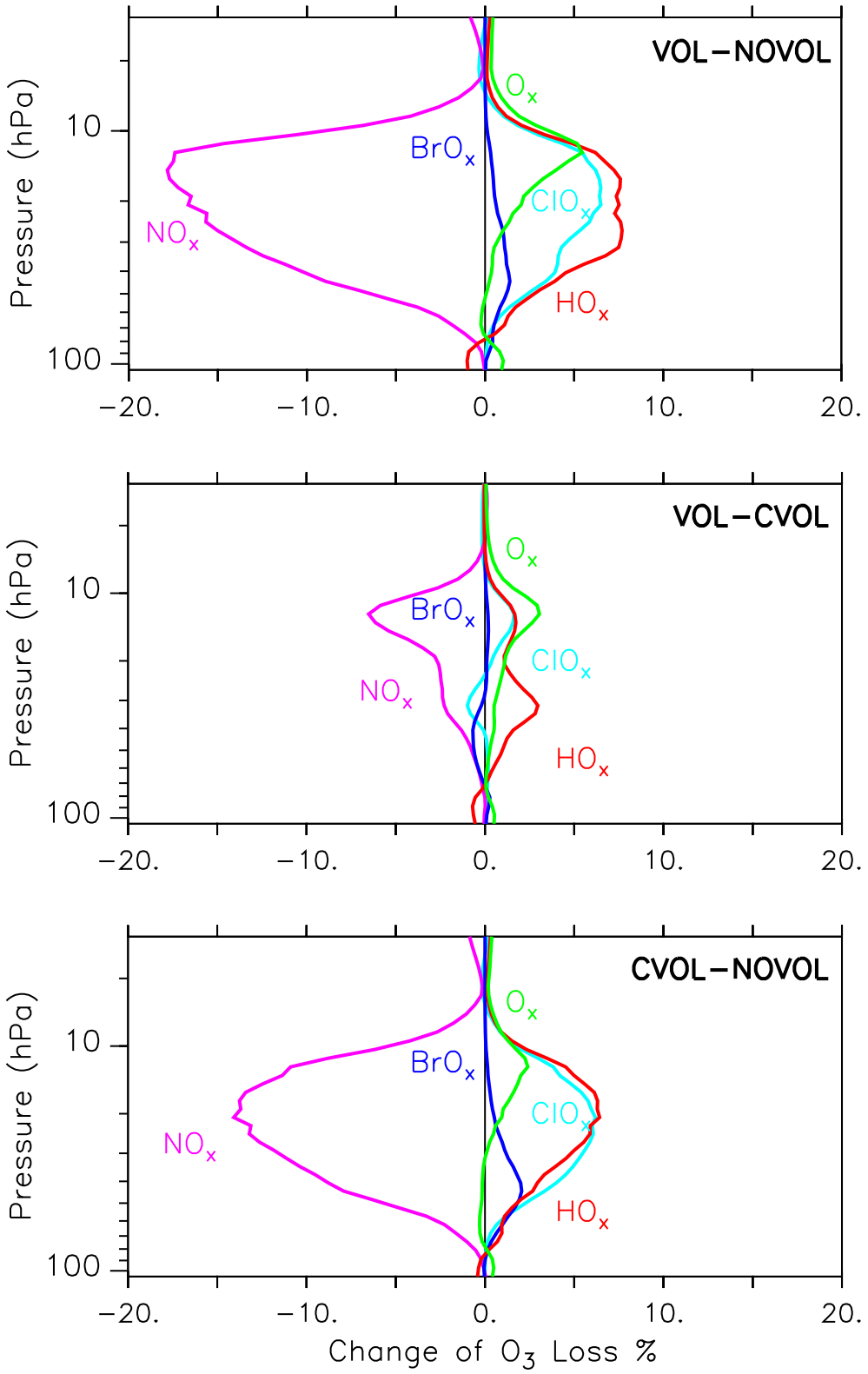

Figure 4.11: Curves show the differences of the relative percentage points (%) for each catalytic ozone loss cycle between VOL - NOVOL, VOL-CVOL and CVOL-NOVOL. These are zonally, monthly (October 1991) and latitudinally averaged between 20° S and 20° N.

4.4 Effects of Volcanic Aerosols on Stratospheric Water Vapour and Methane

4.4.1 Stratospheric Water Vapour

Stratospheric water vapour (SWV) is in the tropics vertically transported from the troposphere beneath. This transport is controlled by the temperature at the tropopause, the so-called cold point temperature. Volcanic aerosols cause a stratospheric heating, which also affects the temperature at the tropopause. Löffler et al. (2016) state that volcanic eruptions lead to higher cold point temperatures at the tropopause and to a subsequent increase of the stratospheric water vapour mixing ratio. For our simulations, this change in SWV is shown in Figure 4.12, with locally up to 25 % more water vapour, which becomes vertically dispersed by time. The tape recorder signal is clearly visible (Mote et al., 1996). In the upper stratosphere, a negative water vapour anomaly between 5 to 40 hPa occurs, up to 5 %. This decrease arises from the volcanic heating, which induces an uplifting of air with lower SWV mixing ratios (Löffler et al., 2016). The negative perturbation is transported to higher altitudes and follows the tape recorder as well.
The pure chemical effect affects SWV, without a heating of the stratosphere, but due to the presence of aerosols. The tropopause level at around 100 hPa cools off 0.4 K, this leads to a reduction of the cold point temperature (Figure 4.1, lower panel). For this reason, the water vapour mixing ratio in the stratosphere decreases by up to 0.2 ppmv, which corresponds to 4 %. This anomaly propagates vertically with time. With the presence of volcanic aerosols, a separate negative anomaly occurs in the middle stratosphere starting in July 1991. In order to understand the origin of the second perturbation, the aggregate state of SWV has to be investigated. The volcanic plume alone provides more condensation nuclei to form droplets (Figure 4.13, upper panel). The volcanic plume causes a phase change of water vapour into liquid and ice. An increase in liquid and ice mixing ratios of H_2O within the volcanic plume, marked as white contours can be observed. By calculating the total water content for the chemical effect, the aggregate phase change disappears and only the reduction of the SWV mixing ratio by the transport, remains. The decrease of water vapour transport lasts for at least 3 years after the eruption. At the end of 1992, a weakening of the negative perturbation starts.
Thus, volcanic aerosols have two opposite effects on SWV. The dominant effect is the volcanic heating with a corresponding increase of SWV, whereas the additional aerosol surface reduces SWV.

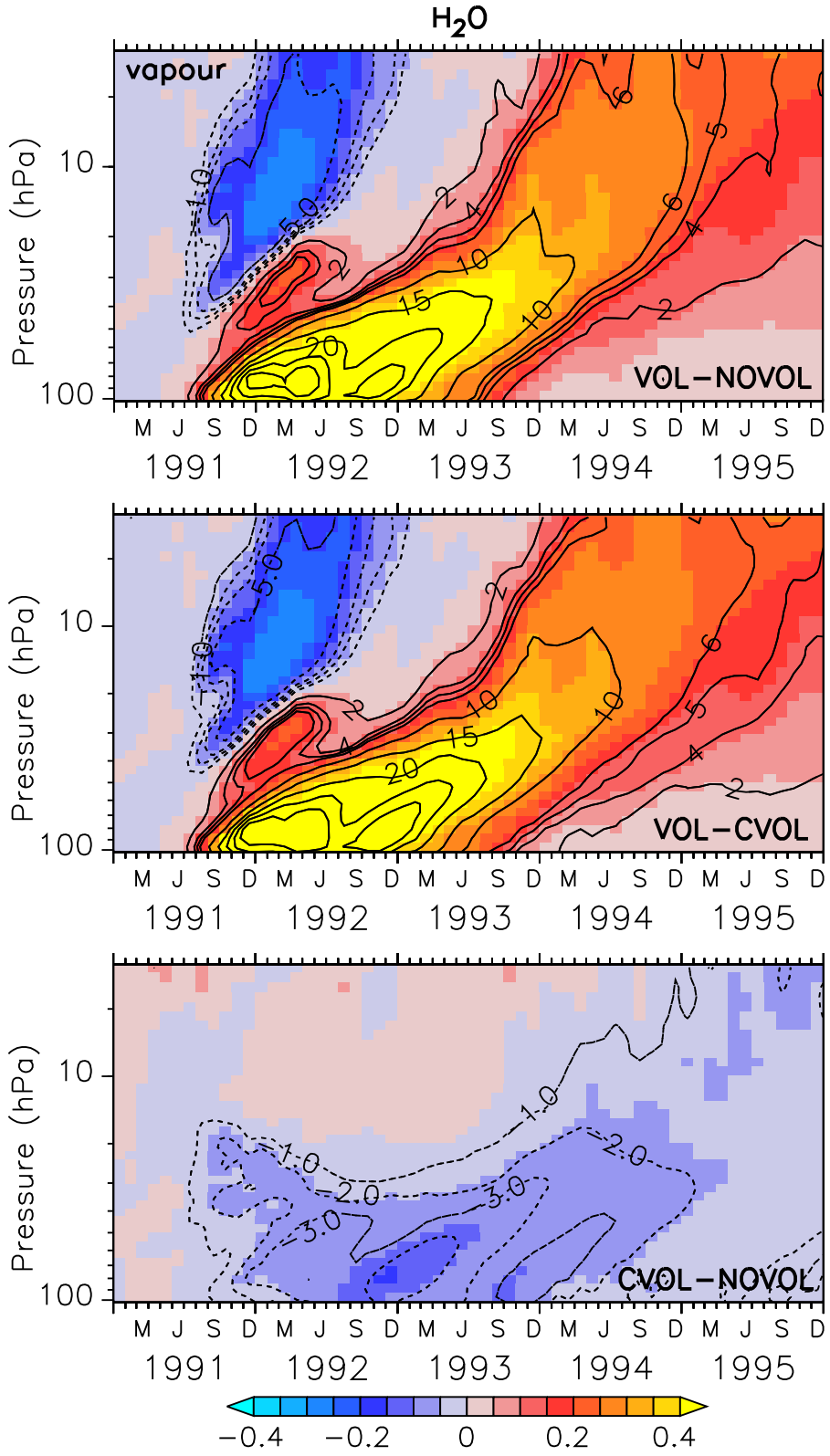

Figure 4.12: Colours show the differences of the mixing ratios (ppmv) of water vapour between the simulations. The black contours show the relative change of H_2O in comparison to NOVOL and CVOL, respectively. Contour intervals are nearly logarithmic with 1, 2 and 5 %. The mixing ratios are monthly, zonally and latitudinally averaged between 20° S and 20° N.

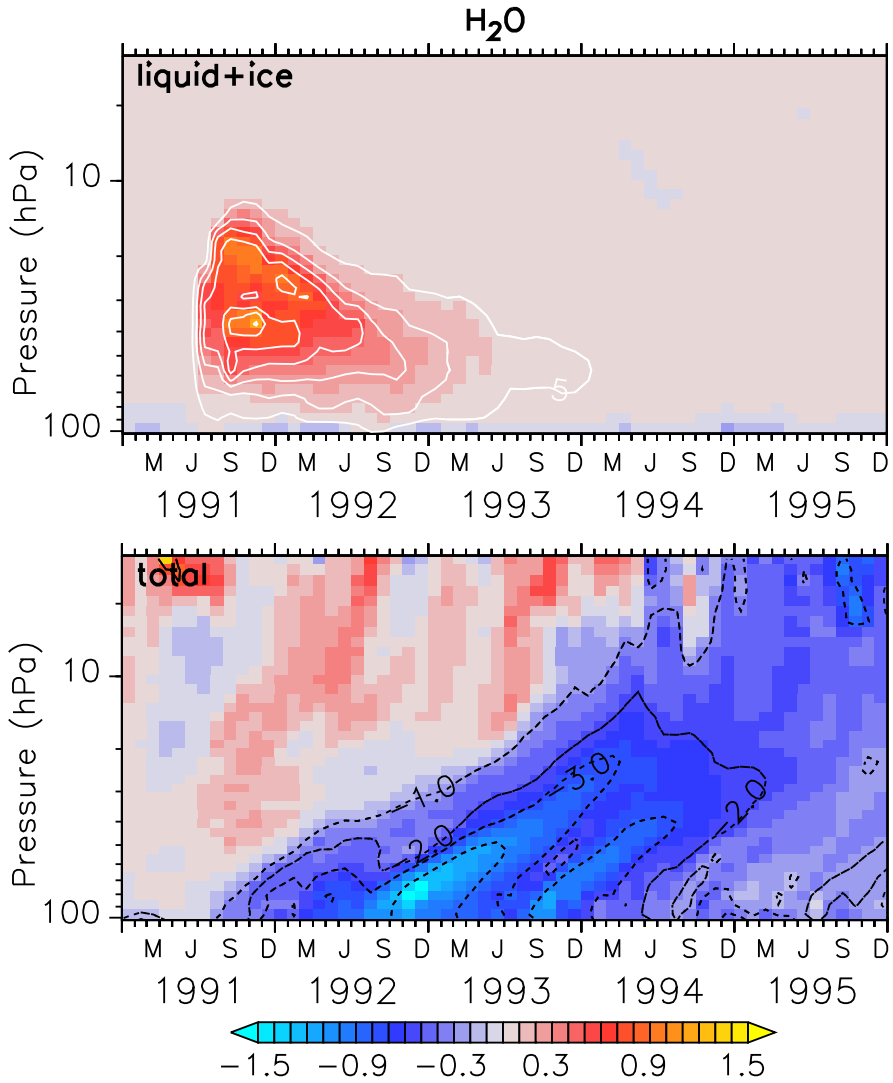

Figure 4.13: Colours show the absolute differences of water content mixing ratios between CVOL - NOVOL of the aggregate states liquid and ice, and the total water content (10^{-7} mol/mol) as zonal and latitudinal averages (20° S and 20° N). Contours indicate the relative change (%). Contour intervals are 1 %. The white contours mark the volcanic plume represented as the liquid aerosol surface area density (10^{-8} cm^2/cm^3) in VOL and CVOL. Here the contour interval is 5 %.

4.4.2 Stratospheric Methane

The methane distribution is also affected by the volcanic eruption. The unperturbed distribution of stratospheric CH_4 decreases with height (Figure E.1). The precursors for methane depletion are H_2O and $O(^1D)$, which produce the hydroxyl radical OH. OH is responsible for 90 % of the methane destruction and determines the lifetime of CH_4 (Chapter 1.5.1).

Already 3 months after the eruption an increase of methane between 40 and beyond 10 hPa can be noticed with changes of more than 80 ppbv, corresponding to a change of 10 % with respect to the absolute methane in the unperturbed simulation NOVOL (Figure

4.14). This anomaly lasts for two years after the eruption. The methane increase is caused by the volcanically induced stratospheric heating and by a reduced methane depletion via OH (central panel). In the lower stratosphere methane slightly changes by 1 %. This arises from a perturbation of OH in the lower stratosphere, which is related to the water vapour increase. Overall, the methane anomaly pattern highly correlates with the anomalies of SWV. Differences of OH indeed do not show a clear pattern, due to the high reactivity and the short lifetime of the hydroxyl radical.

CH_4 is therefore mostly perturbed by the volcanic heating and less affected by the changed chemistry due to the additional aerosol surface.

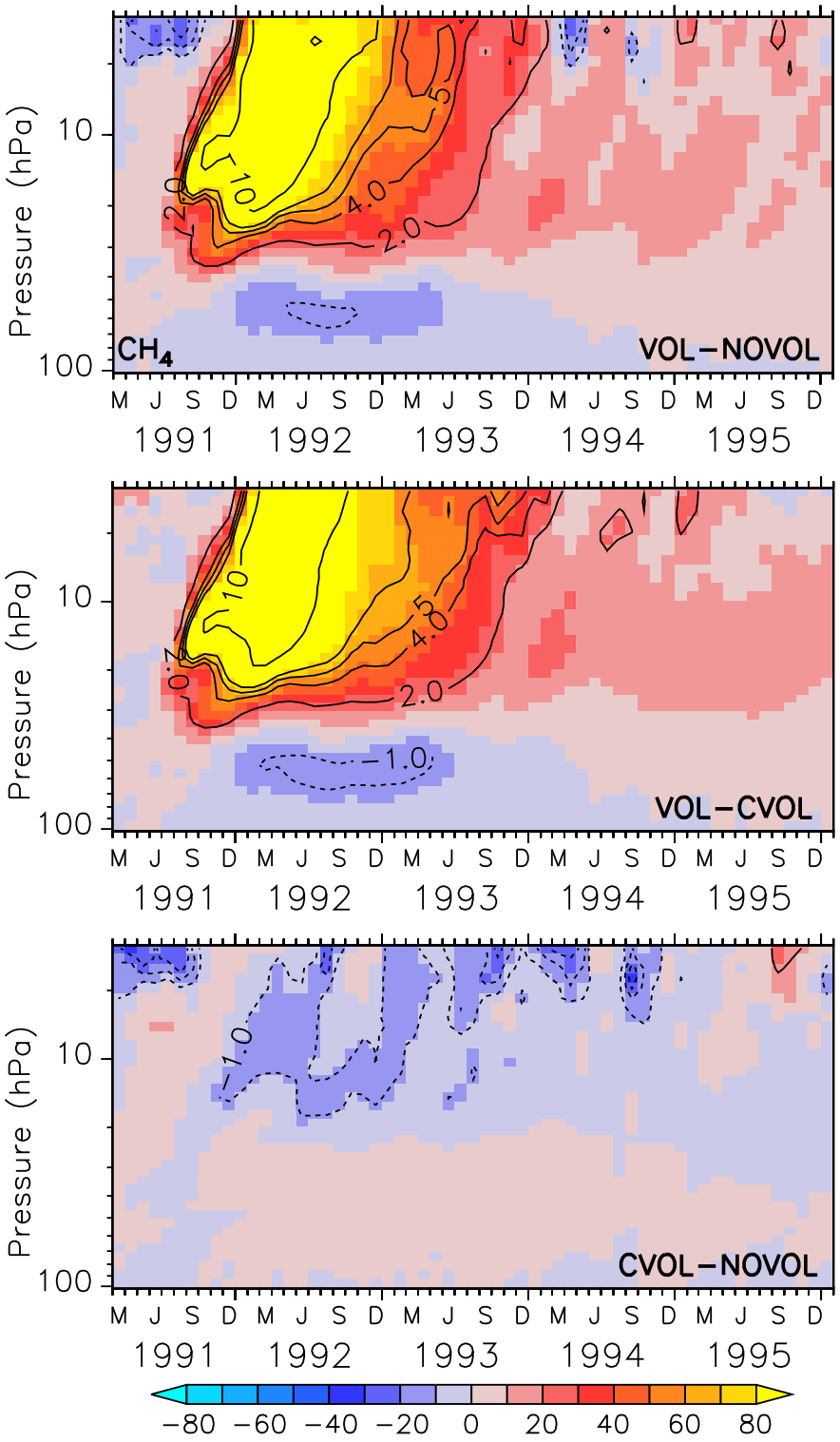

Figure 4.14: Colours show absolute differences of methane mixing ratios (ppbv) between the simulations for 1991-1995. Contours indicate the relative changes (%) of the volcanically induced change in the tropics. The differences are averaged zonally and latitudinally between 20° S - 20° N. Contour intervals are nearly logarithmic with 1 %, 2 % and 5 %.

Chapter 5

Summary and Discussion

5.1 Summary

- Three nudged simulations with volcanic aerosols (VOL), without volcanic aerosols (NOVOL) and without the radiative heating by aerosols (CVOL) are used.
- VOL-NOVOL represents the combined effect on the chemical composition, VOL-CVOL shows the radiative heating by volcanic aerosols and CVOL-NOVOL indicates the pure chemical effect by the larger aerosol surface.
- Stratospheric temperature increase up to 4 K within the volcanic plume due to radiative heating by volcanic aerosols.
- The reduction of the total ozone column is of 6 % and comes primarily from the volcanic heating.
- At 20-50 hPa, the volcanic heating reduces ozone by 0.6 ppmv (10 %).
- The volcanic heating raises the cold point temperature so that the SWV increase by 25 %.
- Tropical methane clearly increases due to the volcanic heating by 10 % above 25 hPa within 2 months after the eruption.
- Between 5-20 hPa, immediately after the eruption, SWV decreases due to an uplift of drier air and limits the availability of OH due to volcanic heating.
- The chemical effect causes a temperature increase of 0.4 K at 10 hPa, but a cooling of 0.4 K in the lower stratosphere.
- However, from the chemical effect alone a slight increase of ozone in the first half year after eruption was found.
- At 10 hPa, the pure chemical effect increases ozone by 0.7 ppmv (4 %) and in the lower stratosphere ozone is reduced by up to 6 %.

- The reduction of NO_x into HNO_3 is primarily due to the larger aerosol surface.
- The NO_x cycle slows down, other catalytic ozone depletion cycles start to compensate the O_3 depletion but do not overcompensate it.

5.2 Discussion

The Mt. Pinatubo eruption in 1991 is one of the most studied volcanic events in terms of climate and chemical forcing. Especially the chemical impacts at the poles have been well investigated, but in the tropics there is still a lack of understanding of the pure chemical impacts. Therefore the present study keeps the focus on the tropical atmosphere between 20° S and 20 ° N. The chemistry climate models to simulate the impacts are getting more and more comprehensive, especially in simulating chemical processes. The chemistry-climate model EMAC has continuously been further developed and is best-suited for sensitivity studies concerning volcanic eruptions.

This section focuses on some selected results from literature, in order to compare the findings of this study. The simulation period of VOL, NOVOL and CVOL is just 9 years, and therefore too short to fully cover the unperturbed interannual variability. We used therefore two other EMAC model simulations, namely RC1-base-07 and RC1SD-base-10, spanning over 50 and 30 years, respectively, to estimate the seasonal cycle and the interannual variability. RC1-base-07 is a free-running simulation from 1960-2011 without volcanic aerosols. RC1SD-base-10 is a nudged simulation, which omit volcanic aerosols as well and is available for the time period 1979-2013.

The author uses the standard deviation σ to put the amplitude of the volcanic signal in comparison to the natural variability. A volcanic signal is defined as strong, when the amplitude exceeds 1 σ. The standard deviation σ_X is defined as the square root of the variance as

$$\sigma_X = \sqrt{Var(X)}, \tag{5.1}$$

where Var(X) denotes the variance of variable X. The variance of X is defined as

$$Var(X) = \frac{1}{n}\sum_{i=1}^{n}(X_i - \overline{X})^2, \tag{5.2}$$

where $\overline{X}$ denotes the empirical mean

$$\overline{X} = \frac{1}{n}\sum_{i=1}^{n} X_i \tag{5.3}$$

with n being the number of values and X_i the value of the variable.

The standard deviation is calculated from the means over all months for the periods 1979-2013 and 1960-2011, respectively. The result is a single value of the standard deviation and is a measure of the natural variability.

5.2.1 Stratospheric Ozone Anomalies

Ozone is considered to be one of the best studied chemical compounds in the stratosphere. Most of the studies are connected to the Mt. Pinatubo eruption are reviews of observational data (e.g. Coffey, 1996). A large number of studies are about volcanically induced changes of O_3 at the poles, but there are few studies regarding the tropics that figured out a decrease of ozone (Angell, 1997a; Dameris et al., 2005). Grant et al. (1992) and Schoeberl et al. (1993) investigated total ozone column depletions of 5-8 % in the tropical region in the 6 months after the Mt. Pinatubo eruption. These result agree with our findings in section 4.3.1 with up to 6 % column loss of O_3 quite well. Coffey (1996) pointed out that studies using ozone satellite observations attributed much of the O_3 anomalies to the QBO (Chandra, 1993; Randel et al., 1995). Angell (1997a) investigated a decrease of the total ozone column of 5-8 % after the Mt. Pinatubo eruption. McCormick et al. (1995) indicated the same order of magnitude from observation data with an ozone loss of 6-8 % over the Equator in the first several months after the eruption. The largest loss of ozone with 20 % could be observed between 24-25 km (25-30 hPa level). This anomaly corresponds spatially to the ozone decrease explained in this study (section 4.3.1).
In the present study, only the order of magnitude of the ozone loss is with 15 % slightly lower than in McCormick's et al. (1995) study. Above 30 km (11 hPa), McCormick et al. (1995) indicated small increases of O_3. This is confirmed by this study, which shows an increase of O_3 at the same height of 5 %. (Section 4.3.1). McCormick et al. (1995) attributed this anomalies to the stratospheric heating and the uplifting of O_3 into altitudes, where photochemical ozone depletion is more effective. Only the ozone increase in the lower stratosphere between 60 and 100 hPa with up to 10 % as presented in section 4.3.1, was not mentioned by any of these studies.

Telford et al. (2009) used two nudged simulations and one free-running simulation to separate the total volcanic effect on the chemistry as in our study similar to VOL-NOVOL. In comparison to Telford et al. (2009), in this study, the total effect consisting of the temperature plus the effect of the larger aerosol surface shows a decrease up to 14 DU (6 %) between 20° S and 20° N. In contrast, Telford et al. (2009) figured out an increase of the combined effect of 2 DU in the first year after the eruption and a reduction of the total ozone column about almost 4 DU starting in the midst of 1992 (10° S - 10° N). This temporary increase of ozone appears in our study with 2 DU as well, but is purely caused by the change of the heterogeneous chemistry due to the larger aerosol surface. The small increase is superimposed by the decrease induced by the radiative volcanic heating so that in sum the total effect is negative immediately after the eruption.

A couple of studies attribute the ozone anomalies primarily to transport effects rather than to chemical effects (Pitari, 1992; Stenke and Grewe, 2005; Aquila et al., 2015). In our study, transport effects arising from the volcanic heating are included in the temperature effect, but we did not analyse this effect in more detail.

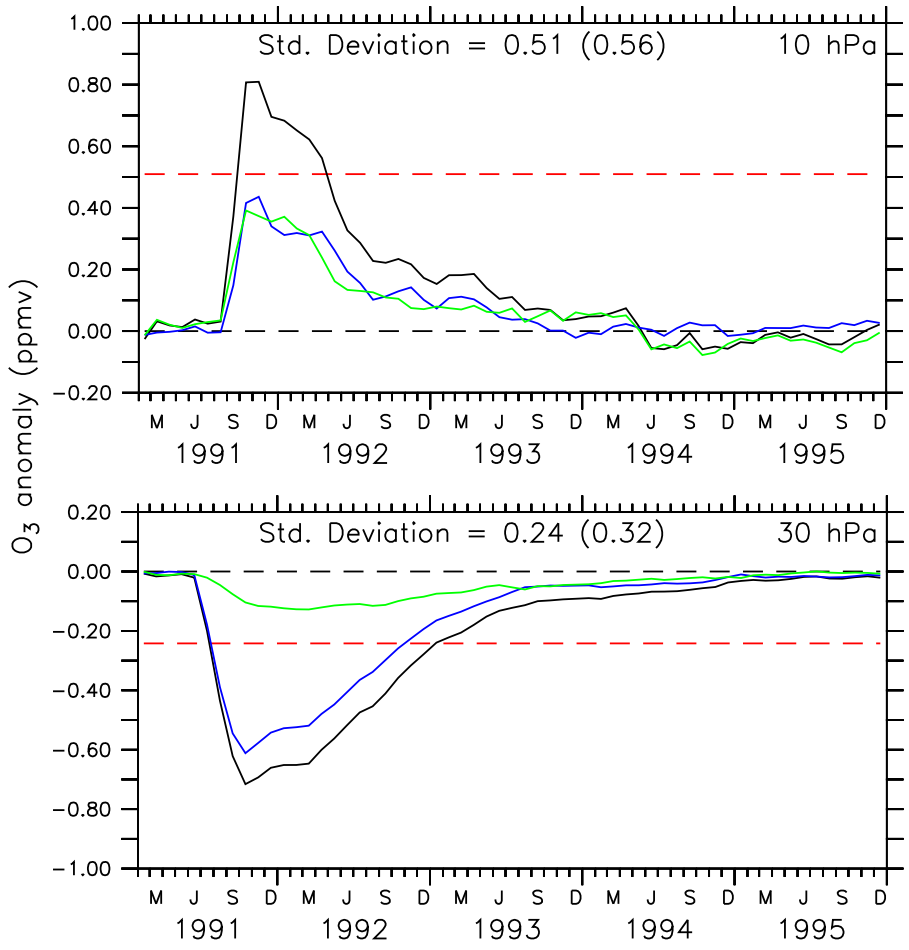

Figure 5.1: The black curves show the time series (1991-1995) of zonally averaged absolute differences (VOL-NOVOL) of O_3 mixing ratios (ppmv) in the tropics (20° S - 20° N) at 10 hPa (upper) and 30 hPa (lower). The blue curves show the contribution of the volcanic heating (VOL-CVOL) and the green curves the contribution of the chemical effect (CVOL-NOVOL). The dashed red line indicates the standard deviation of the ozone mixing ratios in simulation RC1-base-07 over the years 1960-2011. The σ values in the brackets arise from the simulation RC1SD-base-10 (1979-2013).

To assess the amplitude of the volcanic signal in comparison to the interannual variability, Figure 5.1 shows the volcanic O_3 mixing ratio signal (VOL-NOVOL) together with the standard deviation σ of the years 1960-2011 of the free-running simulation RC1SD-base-07 for two heights. Levels are compared at a height of 10 hPa, where the largest increase appears, and at 30 hPa where the strongest ozone loss takes place. In addition, the comparative size of the temperature and chemical effect is assessed. The blue curves show the ozone changes due to volcanic heating and the green curves the ozone anomalies due to the chemistry. The volcanic signal starts in August 1991 and reaches 0.8 ppmv or 1.5 σ in November 1991 at 10 hPa. The volcanic peak is clearly larger than the interannual variability and the seasonal cycle. At 10 hPa both effects contribute equally to the ozone perturbation, but remain below 1 σ, respectively. At 30 hPa, ozone decreases by 0.7 ppmv, roughly 3 σ, in October 1991. Here, the temperature effect (blue) causes the largest ozone anomaly and reaches 2 σ.

The chemical effect is small, and does not reach one half of σ. Consequently, at this height the temperature effect is dominating. The O_3 perturbation is similar at both heights, but the seasonal cycle at 10 hPa is higher. The standard deviation at 30 hPa is only 0.24 ppmv and the half of σ at 10 hPa. In the upper stratosphere the seasonal cycle of O_3 is larger than in the middle stratosphere. The σ values of ozone in the brackets represent a slightly higher standard deviation for the simulation RC1SD-base-10 at both heights (Figure 5.1).

5.2.2 Stratospheric Methane Anomalies

Considine et al. (2001) evaluated with a two- dimensional model the effects of the Mt.Pinatubo eruption on stratospheric methane. The result was an increase of CH_4 of 10 % in the upper stratosphere in early 1992 above 1 hPa, caused by an increase in the tropical upwelling between 20 and 30 hPa by 24 %. Anomalies in methane of the same order of magnitude are derived in the present study already 20 hPa and further up. In comparison to Considine et al. (2001), this study revealed, that the methane increase in the upper stratosphere is not only caused by an increase of the tropical upwelling, but also by a change of SWV. The decrease of SWV at 5-20 hPa arises from an uplift of drier air and reduces the formation of OH. At this point, the increase of CH_4 arises from a chemical process and not from a transport of CH_4 from beneath, because the change patterns correlated. Interestingly, the strong SWV increase in the lower stratosphere does not lower methane, even though OH increases by up to 10 %.
Similar to the previous section, in the following the volcanic signal is compared to the standard deviation of the background variability. Figure 5.2 shows the CH_4 anomalies for the upper stratosphere at 10 hPa and 1 hPa in comparison to σ.

The black curve of the upper panel of Figure 5.2 represents the combined volcanic signal (VOL-NOVOL) at 10 hPa, and follows the well-known methane increase starting in August 1991 (Section 1.5.1). Important is the blue curve (VOL-CVOL), which indicates the increase of CH_4 of 0.14 ppmv in early 1992 due to the volcanic heating. It exceeds 1 σ and is clearly a result of the volcanic eruption, in contrast to the chemical effect, which is represented by the green curve and remains mostly unaffected.
The combined volcanic signal (VOL-NOVOL) of CH_4 is slightly damped by the small decrease due to the pure chemistry. Further up in the stratosphere at 1 hPa, the seasonal cycle of methane is almost halved, and the amplitudes of the volcanic signal decrease. The temperature induced increase of CH_4 occurs shifted by one year in comparison with that at 10 hPa. In December 1992, the volcanic heating signal reaches 1 σ, at the same time the chemical contribution to the methane change decreases. The σ values of methane in the brackets represent at both heights a slightly higher standard deviation in the RC1SD-base-10 simulation (Figure 5.2). In general, the amplitude of the volcanic signal stays within 1σ of the natural variability.

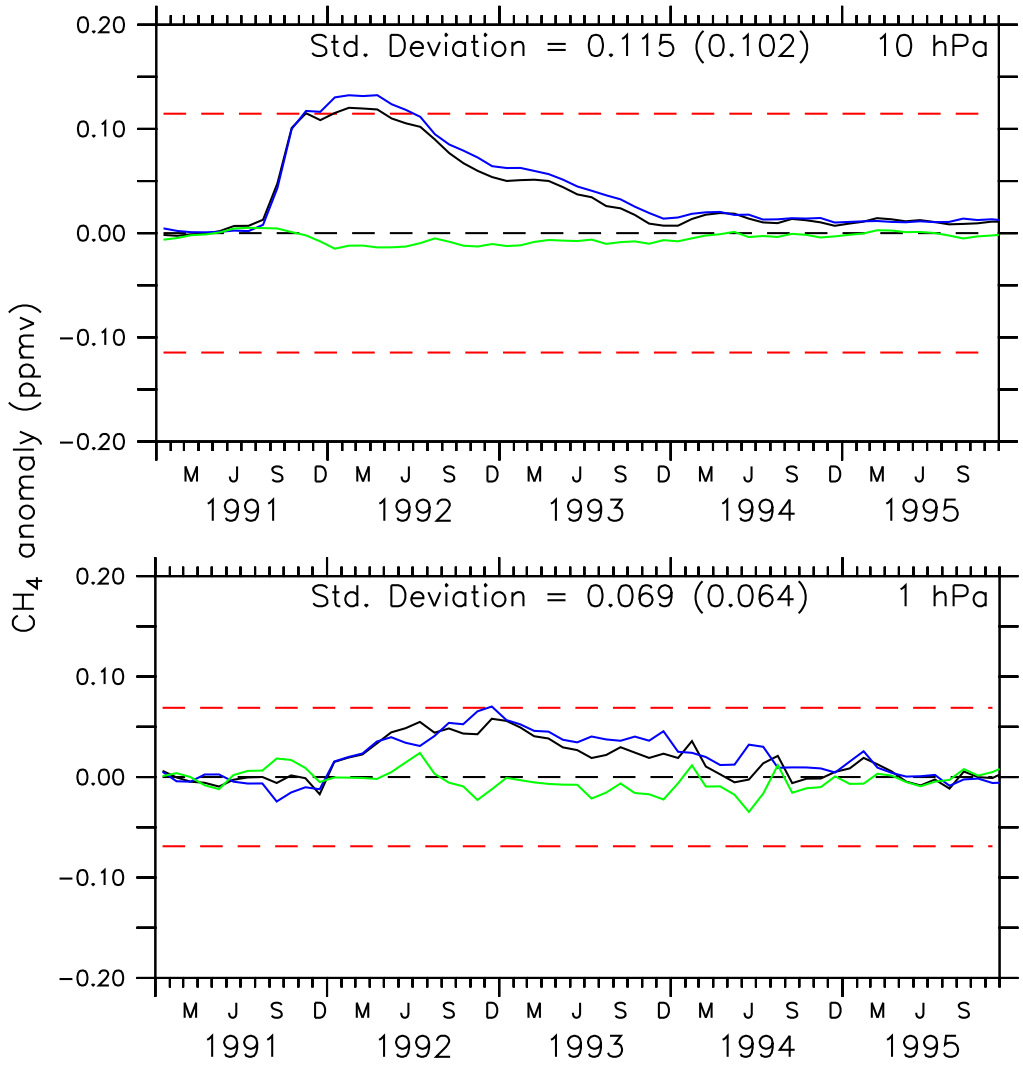

Figure 5.2: The black curves show the time series (1991-1995) of zonally averaged absolute differences (VOL-NOVOL) of CH_4 mixing ratios (ppmv) in the tropics (20° S - 20° N) at 10 hPa (upper) and 1 hPa (lower). The blue curves show the contribution of the volcanic heating (VOL-CVOL) and the green curves the contribution of the chemical effect (CVOL-NOVOL). The dashed red line indicates the standard deviation of the methane mixing ratios in simulation RC1-base-07 over the years 1960-2011. The σ values in the brackets arise from the simulation RC1SD-base-10 (1979-2013).

Chapter 6

Conclusion and Outlook

The goal of this study was to quantify the change in the chemical composition of the atmosphere by the Mt. Pinatubo eruption and to separate the temperature effect from the pure chemical effect. Both effects are proved to be additive and represent in sum the total effect, but both have contrary impacts on the chemical species of the stratosphere.
In general, especially the reduction of the total ozone column in the first 12 months after the eruption is just caused by the volcanic heating. The decrease of ozone between 20 and 50 hPa by up to 15 % is primarily caused by the temperature effect and the related enhancement of the vertical ascent, which displaces the ozone maximum. During the same period, the chemical effect slightly increases the ozone column. This ozone increase takes place at 10 hPa and is primarily caused by the larger aerosol surface in other words, by the slow down of the NO_x cycle. Overall, both effects are contrary, but lead to a reduction of the ozone column by 6 %.
The decrease of stratospheric water vapour by 5 % between 5-40 hPa reduces OH and causes an increase of CH_4 by up to 10 % at this height. In contrast, the strong SWV increase starting in the lower stratosphere immediately after eruption, does not affect the methane levels. The positive SWV perturbation fully arises from the volcanic heating of the tropopause but is damped by the pure chemical effect, which cools the lower stratosphere. In conclusion, both effects having contrary influence on the chemical species of the stratosphere.

However, there are still questions left to be answered. The volcanic forcing is prescribed as volcanic aerosols derived from satellite measurements. A further development could be, using an interactive stratospheric aerosol submodel. Furthermore, in the present simulations volcanic emissions of other species are completely omitted, so that CO_2 and H_2O are potentially systematically underestimated. Especially water vapour contributes largely to the composition of the volcanic emitted gases. Admittedly, quantifying volcanic emissions, especially of past eruptions, is still problematic. Nevertheless, the other volcanic gases (e.g. H_2O, CO_2) affect the chemical reactions and the related ozone and methane budget possibly to a considerable extent. An expansion to quantify volcanic emissions could lead to an improved understanding of how volcanoes contribute to the chemical reactions in the stratosphere and modify the chemical composition. A further limitation

is that the perturbation of ozone arises from a temperature induced enhancement of the transport and the heterogeneous chemistry. Both effects are included in VOL-CVOL, but can not be separated. Another inaccuracy are the simulated photolysis rates, which are not directly affected by the extinction of the solar radiation due to volcanic aerosols. Hence the ozone production is systematical overestimated in simulation VOL and CVOL.
The applied nudging technique reduces the noise when the simulations are compared because the same synoptic condition is forced by the nudging. However, nudging limits the analysis of dynamical changes. A further expansion could be to conduct EMAC simulations in free-running mode and to generate an ensemble with the same boundary conditions. Out of these ensemble, statistical analyses would be possible to study the change in dynamics. In this study the focus was on the tropics. Extending the analysis to the mid latitudes and the polar regions, a quantification of the volcanic heating (VOL-CVOL) and the chemical forcing (CVOL-NOVOL) in these regions would be possible. The impact of the volcano on the formation of the PSC's could be a focus of future work related to this topic.

Overall, this study contributes to the knowledge about volcanic perturbations in the tropics, especially regarding the separation of the temperature and the chemical effect. It shows how contrary the temperature affects the chemical composition of the stratosphere in comparison to the larger aerosol surface. In terms of the increasing importance of climate research, natural climate forcings such as volcanic eruptions will remain in the focus of future research.

Data Availability

The data, the present study is based on, are stored at the Deutsches Klimarechenzentrum (DKRZ) in Hamburg and are available from the corresponding author, Markus Kilian, upon request.

Acknowledgement

At this point, I want to thank my supervisors Dr. Sabine Brinkop and Dr. Patrick Jöckel for their trust to let me work on this project. Your support in difficult questions concerning the model was charaterised by engagement and endurance. I could ask you anytime and you took the time for a constructive discussion. A special thanks to Sabine for being such a kind and humorous supervisor and for the hours and hours we spent in your office just to understand new chemical results. Patrick, you are not just a great scientist, but you really have the gift of endurance and encouragement, and you are see the person behind your colleague. Keep it up. Although sometimes the topic was difficult, I developed more and more interest. After understanding the background information in a better way, I really liked the project and enjoyed to investigate all those findings. A big thanks to my supervisor Dr. Fabien Maussion at the Leopold-Franzens-Universität Innsbruck of the Department of Atmospheric and Cryospheric Sciences (ACINN), who made it possible to write my Master thesis in cooperation with the German Aerospace Center in Oberpfaffenhofen. Thank you for your open-minded thinking.

In addition, I want to thank my colleagues at the department for the support and constructive approaches concerning my questions.

Moreover, I want to thank my family for their support. Especially a big thanks to my parents who always encouraged me all these years to end up at this last step before my graduation.

Last but not least, I owe God all good things in my life. He made everything possible and holds my future in his hands. Thank you for your faithfulness, your goodness, your hope and your favour.

"Commit to the Lord whatever you do,
and your plans will succeed."
(Proverbs 16,3)

Appendix A

Absolute mixing ratio of NO_x

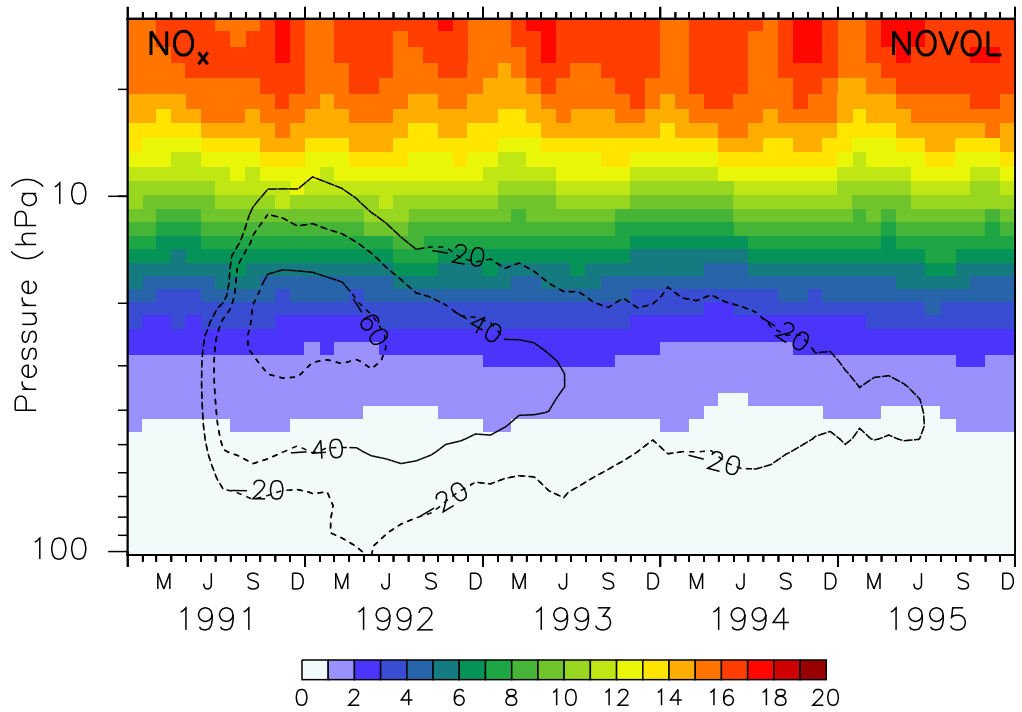

Figure A.1: Colours show the absolute mixing ratios (ppbv) of NO_x for the unperturbed case NOVOL. The black contours show the relative change of NO_x (%) in VOL in comparison to NOVOL. The contour interval is 20 %. The mixing ratios are monthly, zonally and latitudinally averaged between 20° S and 20° N.

Appendix B

Absolute mixing ratio of ClO_x

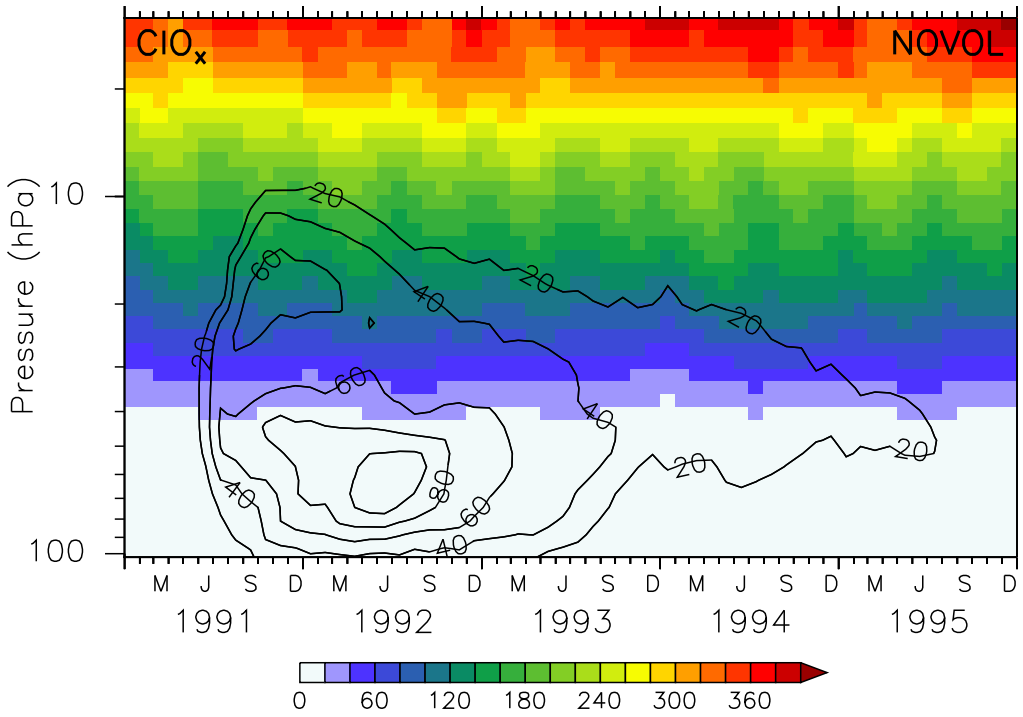

Figure B.1: Colours show the absolute mixing ratios (pptv) of ClO_x for the unperturbed case NOVOL. The black contours show the relative change of ClO_x (%) in VOL in comparison to NOVOL. The contour interval is 20 %. The mixing ratios are monthly, zonally and latitudinally averaged between 20° S and 20° N.

Appendix C

Absolute mixing ratio of BrO_x

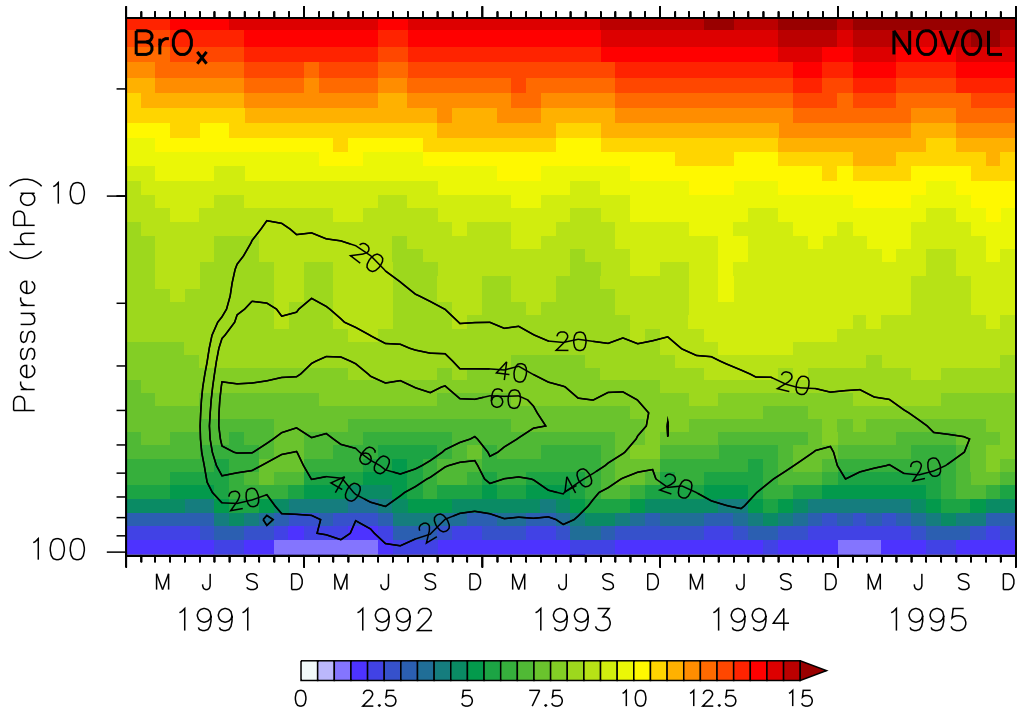

Figure C.1: Colours show the absolute mixing ratios (pptv) of BrO_x for the unperturbed case NOVOL. The black contours show the relative change of BrO_x (%) in VOL in comparison to NOVOL. The contour interval is 20 %. The mixing ratios are monthly, zonally and latitudinally averaged between 20° S and 20° N.

Appendix D

Absolute mixing ratio of HO_x

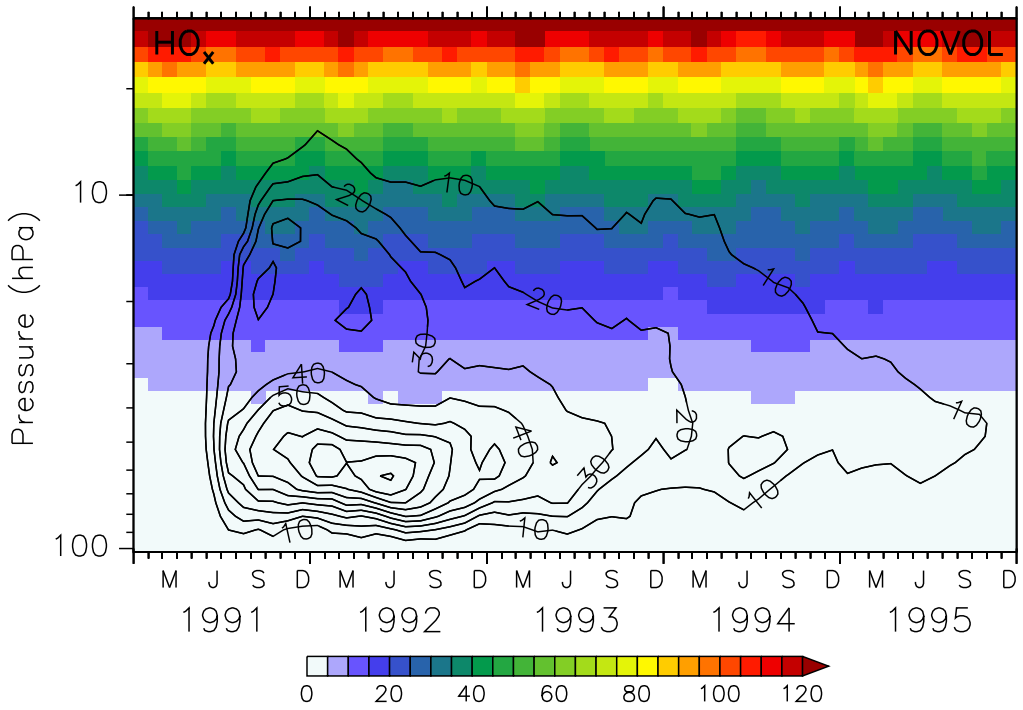

Figure D.1: Colours show the absolute mixing ratios (pptv) of HO_x for the unperturbed case NOVOL. The black contours show the relative change of HO_x (%) in VOL in comparison to NOVOL. The contour interval is 10 %. The mixing ratios are monthly, zonally and latitudinally averaged between 20° S and 20° N.

Appendix E

Absolute Distribution and Relative Perturbation of CH_4

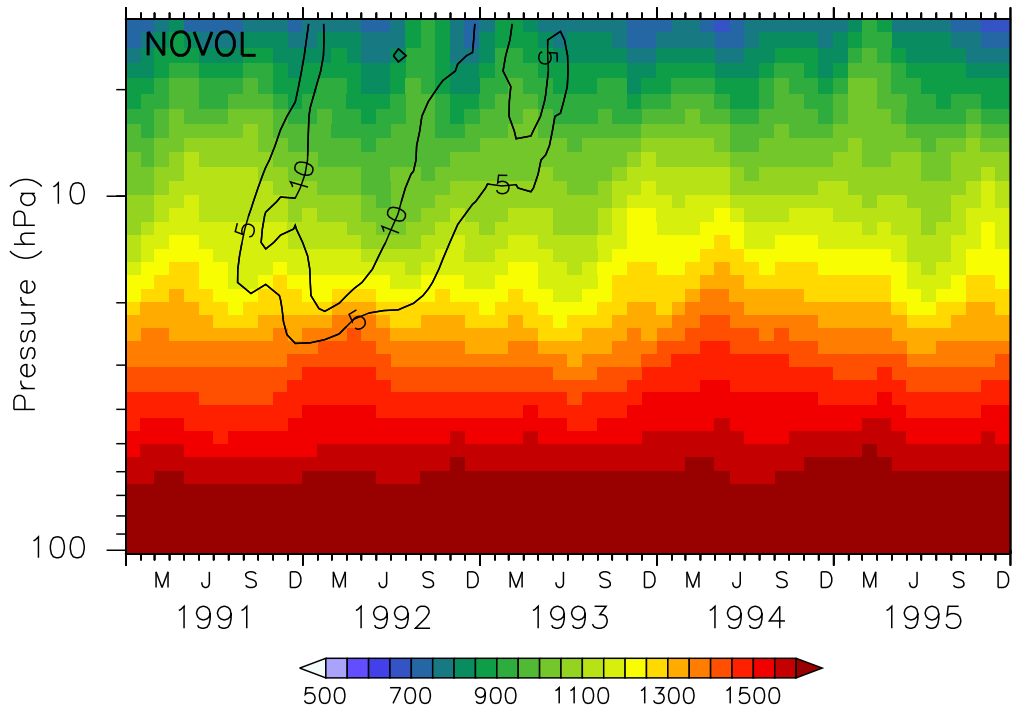

Figure E.1: Colours show the absolute mixing ratios (ppbv) of CH_4 for the unperturbed case NOVOL. The black contours show the relative change of methane (%) in VOL in comparison to NOVOL. The contour interval is 5 %. The mixing ratios are monthly, zonally and latitudinally averaged between 20° S and 20° N.

References

Angell, J., 1997a: Estimated impact of agung, el chichon, and pinatubo volcanic eruptions on global and regional total ozone after adjustment for the qbo. *Geophysical Research Letters*, **24**, 647–650.

Aquila, V., L. D. Oman, R. Stolarski, A. R. Douglass, and P. A. Newman, 2013: The response of ozone and nitrogen dioxide to the eruption of mt. pinatubo at southern and northern midlatitudes. *Journal of the Atmospheric Sciences*, **70 (3)**, 894–900, doi:10.1175/JAS-D-12-0143.1, URL https://doi.org/10.1175/JAS-D-12-0143.1, https://doi.org/10.1175/JAS-D-12-0143.1.

Atkins, P., and J. De Paula, 2006: *Atkins' Physical chemistry*. Oxford University Press.

Bates, D. R., and M. Nicolet, 1950: The photochemistry of atmospheric water vapor. *Journal of Geophysical Research*, **55 (3)**, 301–327, doi:10.1029/JZ055i003p00301, URL https://agupubs.onlinelibrary.wiley.com/doi/abs/10.1029/JZ055i003p00301, https://agupubs.onlinelibrary.wiley.com/doi/pdf/10.1029/JZ055i003p00301.

Benkovitz, M., and other authors, 1996: Global gridded inventories of anthropogenic emissions of sulfur and nitrogen. *J. Geophys. Res.*, **101**.

Cicerone, R., and R. Stolarski, 1974: Stratospheric chlorine: A possible sink for ozone. *Canadian Journal of Chemistry*, **52**, 1610, doi:10.1139/v74-233.

Coffey, M., 1996: Observations of the impact of volcanic activity on stratospheric chemistry. *Journal of Geophysical Research: Atmospheres*, **101 (D3)**, 6767–6780, doi:10.1029/95JD03763, URL https://agupubs.onlinelibrary.wiley.com/doi/abs/10.1029/95JD03763, https://agupubs.onlinelibrary.wiley.com/doi/pdf/10.1029/95JD03763.

Considine, D., Rosenfield, J.E., and J. Fleming, 2001: An interactive model study of the influence of the mount pinatubo aerosol on stratospheric methane and water trends. *Journal of Geophysical Research: Atmospheres*, **106**, 27 711–27 727, doi:10.1029/2001JD000331, URL https://agupubs.onlinelibrary.wiley.com/doi/abs/10.1029/2001JD000331, https://agupubs.onlinelibrary.wiley.com/doi/pdf/10.1029/2001JD000331.

Crutzen, P. J., 1970: The influence of nitrogen oxides on the atmospheric ozone content. *Quarterly Journal of the Royal Meteorological Society*, **96 (408)**, 320–325, doi:10.1002/qj.49709640815.

Dameris, M., and Coauthors, 2005: Long-term changes and variability in a transient simulation with a chemistry-climate model employing realistic forcing. *Atmospheric Chemistry and Physics*, **5 (8)**, 2121–2145, doi:10.5194/acp-5-2121-2005, URL https://www.atmos-chem-phys.net/5/2121/2005/.

Davidson, E., and W. Kingerlee, 1997: A global inventory of nitric oxide emissions from soils. *Nutrient Cycling in Agroecosystems*, **48**, 37–50.

Davis, S. M., and Coauthors, 2016: The stratospheric water and ozone satellite homogenized (swoosh) database: a long-term database for climate studies. *Earth System Science Data*, **8 (2)**, 461–490, doi:10.5194/essd-8-461-2016, URL https://www.earth-syst-sci-data.net/8/461/2016/.

Dee, D. P., and Coauthors, 2011: The era-interim reanalysis: configuration and performance of the data assimilation system. *Quarterly Journal of the Royal Meteorological Society*, **137 (656)**, 553–597, doi:10.1002/qj.828, URL http://dx.doi.org/10.1002/qj.828.

Ehhalt, D. H., 1967: Methane in the atmosphere. *Journal of the Air Pollution Control Association*, **17 (8)**, 518–519, doi:10.1080/00022470.1967.10469012, URL https://doi.org/10.1080/00022470.1967.10469012, https://doi.org/10.1080/00022470.1967.10469012.

Farman, J., B. G. Gardiner, and J. Shanklin, 1985: Large losses of total ozone in Antarctica reveal seasonal ClOx/NOx interaction. *Nature*, **315**, 207–210, doi:10.1038/315207a0.

Grant, W. B., and Coauthors, 1992: Observations of reduced ozone concentrations in the tropical stratosphere after the eruption of mt. pinatubo. *Geophysical Research Letters*, **19 (11)**, 1109–1112, doi:10.1029/92GL01153, URL http://dx.doi.org/10.1029/92GL01153.

Hossaini, R., and Coauthors, 2012: The contribution of natural and anthropogenic very short-lived species to stratospheric bromine. *Atmospheric Chemistry and Physics*, **12 (1)**, 371–380, doi:10.5194/acp-12-371-2012, URL https://www.atmos-chem-phys.net/12/371/2012/.

Jöckel, P., and Coauthors, 2010: Development cycle 2 of the modular earth submodel system (messy2). *Geoscientific Model Development*, **3 (2)**, 717–752, doi:10.5194/gmd-3-717-2010, URL https://www.geosci-model-dev.net/3/717/2010/.

Jöckel, P., and Coauthors, 2016: Earth system chemistry integrated modelling (escimo) with the modular earth submodel system (messy) version 2.51. *Geoscientific Model Development*, **9 (3)**, 1153–1200, doi:10.5194/gmd-9-1153-2016, URL https://www.geosci-model-dev.net/9/1153/2016/.

Labitzke, K., and M. P. McCormick, 1992: Stratospheric temperature increases due to pinatubo aerosols. *Geophysical Research Letters*, **19 (2)**, 207–210, doi:10.1029/91GL02940, URL http://dx.doi.org/10.1029/91GL02940.

Landgraf, J., and P. J. Crutzen, 1998: An efficient method for online calculations of photolysis and heating rates. *Journal of Atmospheric Sciences, v.55, 863-878 (1998)*, **55**.

Levine, I., 1995: *Physical Chemistry*. McGraw-Hill, New York.

Lovelock, E. J., 1971: Atmospheric fluorine compounds as indicators of air movements. *Nature*, **230**, 379.

Löffler, M., S. Brinkop, and P. Jöckel, 2016: Impact of major volcanic eruptions on stratospheric water vapour. *Atmospheric Chemistry and Physics*, **16 (10)**, 6547–6562, doi:10.5194/acp-16-6547-2016, URL https://www.atmos-chem-phys.net/16/6547/2016/.

Mccormick, M., L. W. Thomason, and C. R. Trepte, 1995: Atmospheric effects of the mt pinatubo eruption. *Nature*, **373**, 399–404.

Middlebrook, A., and M. Tolbert, 2000: *Stratospheric Ozone Depletion*. Global change instruction program, University Science Books, URL https://books.google.at/books?id=nT-LQgAACAAJ.

Molina, M. J., and F. S. Rowland, 1974: Stratospheric sink for chlorofluoromethanes: chlorine atom-catalysed destruction of ozone. *Nature*, **249**, 810–812, doi:10.1038/249810a0.

Mote, P., and Coauthors, 1996: An atmospheric tape recorder: The imprint of tropical tropopause temperatures on stratospheric water vapor. *Journal of Geophysical Research Atmospheres*, **101**.

Muthers, S., F. Arfeuille, C. C. Raible, and E. Rozanov, 2015: The impacts of volcanic aerosol on stratospheric ozone and the northern hemisphere polar vortex: separating radiative-dynamical changes from direct effects due to enhanced aerosol heterogeneous chemistry. *Atmospheric Chemistry and Physics*, **15 (20)**, 11 461–11 476, doi:10.5194/acp-15-11461-2015, URL https://www.atmos-chem-phys.net/15/11461/2015/.

Nobel Media, A., 2014: The nobel prize in chemistry 1995. *Nobelprize*, URL http://www.nobelprize.org/nobel_prizes/chemistry/laureates/1995/.

Pitari, G., 1993: A numerical study of the possible perturbation of stratospheric dynamics due to pinatubo aerosols: Implications for tracer transport. *Journal of the Atmospheric Sciences*, **50 (15)**, 2443–2461, doi:10.1175/1520-0469(1993)050<2443:ANSOTP>2.0.CO;2, URL https://doi.org/10.1175/15200469(1993)050<2443:ANSOTP>2.0.CO;2, https://doi.org/10.1175/1520-0469(1993)050<2443:ANSOTP>2.0.CO;2.

Poole, L., and M. Mccormick, 1988: Polar stratospheric clouds and the antarctic ozone hole. *Journal of Geophysical Research*, **93**.

Price, C., J. Penner, and M. Prather, 1997a: Constraints from the global atmospheric electric circuit. *J. Geophys. Res.*, **102**, 5943—-5951, doi:10.1029/96JD02551.

Randel, W. J., F. Wu, J. M. R. III, J. W. Waters, and L. Froidevaux, 1995: Ozone and temperature changes in the stratosphere following the eruption of mount pinatubo. *Journal of Geophysical Research: Atmospheres*, **100 (D8)**, 16 753–16 764, doi: 10.1029/95JD01001, URL https://agupubs.onlinelibrary.wiley.com/doi/abs/10.1029/95JD01001, https://agupubs.onlinelibrary.wiley.com/doi/pdf/10.1029/95JD01001.

Revell, L. E., A. Stenke, B. Luo, S. Kremser, E. Rozanov, T. Sukhodolov, and T. Peter, 2017: Impacts of mt pinatubo volcanic aerosol on the tropical stratosphere in chemistry–climate model simulations using ccmi and cmip6 stratospheric aerosol data. *Atmospheric Chemistry and Physics*, **17 (21)**, 13 139–13 150, doi:10.5194/acp-17-13139-2017, URL https://www.atmos-chem-phys.net/17/13139/2017/.

Robock, A., 2000: Volcanic eruptions and climate. *Reviews of Geophysics*, **38 (2)**, 191–219, doi:10.1029/1998RG000054, URL http://dx.doi.org/10.1029/1998RG000054.

Roeckner, E., and Coauthors, 2006: Sensitivity of simulated climate to horizontal and vertical resolution in the echam5 atmosphere model. *Journal of Climate*, **19 (16)**, 3771–3791, doi:10.1175/JCLI3824.1.

Rowland, F. S., and M. J. Molina, 1994: Ozone depletion: 20 years after the alarm. *Chemical and Engineering News*, **72**, 8–13.

S., C., 1993: Changes in stratospheric ozone and temperature due to the eruptions of mt. pinatubo. *Geophysical Research Letters*, **20 (1)**, 33–36, doi:10.1029/92GL03013, URL https://agupubs.onlinelibrary.wiley.com/doi/abs/10.1029/92GL03013, https://agupubs.onlinelibrary.wiley.com/doi/pdf/10.1029/92GL03013.

Schoeberl, M., P. Bhartia, E. Hilsenrath, and O. Torres, 1993: Tropical ozone loss following the eruption of mt. pinatubo. *Geophysical Research Letters*, **20**, 29–32.

Schumann, U., and H. Huntrieser, 2007: The global lightning-induced nitrogen oxides source. *Atmospheric Chemistry and Physics*, **7 (14)**, 3823–3907, doi:10.5194/acp-7-3823-2007, URL https://www.atmos-chem-phys.net/7/3823/2007/.

Seinfeld, J., and S. Pandis, 1998: *Atmospheric chemistry and physics: from air pollution to climate change*. A Wiley interscience publication, Wiley, URL https://books.google.de/books?id=lK8PAQAAMAAJ.

Self, S., J.-X. Zhao, R. E. Holasek, R. C. Torres, and A. J. King, 1999: The atmospheric impact of the 1991 mount pinatubo eruption. *pubs*.

Shao, A., C. Qiu, X. Wang, and Y. Zhang, 2016: Using the newtonian relaxation technique in numerical sensitivity studies. *Science China Earth Sciences*, **59 (12)**, 2454–2462, doi:10.1007/s11430-016-0033-3, URL https://doi.org/10.1007/s11430-016-0033-3.

Solomon, S., 1999: Stratospheric ozone depletion: A review of concepts and history. *Reviews of Geophysics*, **37 (3)**, 275–316, doi:10.1029/1999RG900008, URL http://dx.doi.org/10.1029/1999RG900008.

Stenke, A., and V. Grewe, 2005: Simulation of stratospheric water vapor trends: impact on stratospheric ozone chemistry. *Atmospheric Chemistry and Physics*, **5 (5)**, 1257–1272, doi:10.5194/acp-5-1257-2005, URL https://www.atmos-chem-phys.net/5/1257/2005/.

T. Simarski, L., 1992: Agu report on volcanism and climate targets media. *Eos, Transactions American Geophysical Union*, **73**, 236–236.

Telford, P., P. Braesicke, O. Morgenstern, and J. Pyle, 2009: Reassessment of causes of ozone column variability following the eruption of mount pinatubo using a nudged ccm. *Atmospheric Chemistry and Physics*, **9 (13)**, 4251–4260, doi:10.5194/acp-9-4251-2009, URL https://www.atmos-chem-phys.net/9/4251/2009/.

Textor, C., H.-F. Graf, C. Timmreck, and A. Robock, 2004: Emissions from volcanoes. *Emissions of Atmospheric Trace Compounds*, C. Granier, P. Artaxo, and C. E. Reeves, Eds., Springer Netherlands, Dordrecht, 269–303.

Thomas, M. A., M. A. Giorgetta, C. Timmreck, H.-F. Graf, and G. Stenchikov, 2009: Simulation of the climate impact of mt. pinatubo eruption using echam5“ part 2: Sensitivity to the phase of the qbo and enso. *Atmospheric Chemistry and Physics*, **9 (9)**, 3001–3009, doi:10.5194/acp-9-3001-2009, URL https://www.atmos-chem-phys.net/9/3001/2009/.

Tie, X., G. P. Brasseur, B. Briegleb, and C. Granier, 1994: Two-dimensional simulation of pinatubo aerosol and its effect on stratospheric ozone. *Journal of Geophysical Research: Atmospheres*, **99 (D10)**, 20 545–20 562, doi:10.1029/94JD01488, URL http://dx.doi.org/10.1029/94JD01488.

von Glasow, R., N. Bobrowski, and C. Kern, 2009: The effects of volcanic eruptions on atmospheric chemistry. *Chemical Geology*, **263 (1)**, 131 – 142, doi:https://doi.org/10.1016/j.chemgeo.2008.08.020, URL http://www.sciencedirect.com/science/article/pii/S0009254108003756, halogens in Volcanic Systems and Their Environmental Impacts.

Wang, Y., A. DeSilva, G. Goldenbaum, and R. Dickerson, 1998a: Nitric oxide production by simulated lightning: Dependence on current, energy, and pressure. *J. Geophys. Res.*, **103**, 149–159.

Wuebbles, D. J., and K. Hayhoe, 2002: Atmospheric methane and global change. *Earth-Science Reviews*, **57 (3)**, 177 – 210, doi:https://doi.org/10.1016/S0012-8252(01)00062-9, URL http://www.sciencedirect.com/science/article/pii/S0012825201000629.

Declaration of Authorship

I,
Markus Kilian,
hereby declare, that the thesis at hand is entirely my own original work except where it is otherwise indicated. I have not used any external sources other than the ones clearly attributed. Furthermore, I certify that neither this thesis nor any part of it has been previously submitted for a degree or any other qualification.

Innsbruck, June 15, 2018 .....

Markus Kilian